

## A study of Ni/La-Al<sub>2</sub>O<sub>3</sub> catalysts: a competitive system for CO<sub>2</sub> Methanation

Gabriella Garbarino<sup>1,2\*</sup>, Chongyang Wang<sup>2</sup>, Tullio Cavattoni<sup>3</sup>, Elisabetta Finocchio<sup>1</sup>, Paola Riani<sup>4</sup>, Maria Flytzani-Stephanopoulos<sup>2</sup> and Guido Busca<sup>1</sup>

- 1 Università degli Studi di Genova, Dipartimento di Ingegneria Civile, Chimica e Ambientale (DICCA), Laboratorio di chimica delle superfici e catalisi, Via Opera Pia 15, 16146 Genova, Italy
- 2 Department of Chemical and Biological Engineering, Tufts University, Medford, MA, USA
- 3 Università degli Studi di Genova, Dipartimento di Chimica e Chimica Industriale (DCCI), Via Dodecaneso, 31 16146 Genova, Italy
- 4 Università degli Studi di Genova, Dipartimento di Farmacia, Viale Cembrano 4, 16147 Genova, Italy

\*phone +390103536029; fax +390103532586; e-mail: [Gabriella.Garbarino@unige.it](mailto:Gabriella.Garbarino@unige.it)

Keywords: Nickel catalysts; Lanthana; alumina-supported catalysts; CO<sub>2</sub> methanation; hydrogenation.

Abstract.

Ni/La- $\gamma$ -Al<sub>2</sub>O<sub>3</sub> samples containing 13.6 wt.% Ni and a variable amount of lanthana (0, 4, 14 and 37 wt.%) were prepared by incipient wetness impregnation, using silica-free  $\gamma$ -Al<sub>2</sub>O<sub>3</sub> support. The materials were characterized, as such or after reaction, with XRD, H<sub>2</sub>-TPR, IR, UV-vis-NIR, XPS and FE-SEM techniques. They were tested as catalysts for CO<sub>2</sub> methanation at atmospheric pressure at GHSV 55000 h<sup>-1</sup>. The reaction is under kinetic control at T < 650-673 K, while the product mixture is under thermodynamic control above this temperature range. Lanthanum addition strongly increases the activity of Ni/ $\gamma$ -Al<sub>2</sub>O<sub>3</sub> for CO<sub>2</sub> methanation. Methane selectivity is increased to nearly 100% at low temperatures, where the reaction is in a kinetically controlled regime (T < 650K). The CO<sub>2</sub> methanation reaction on La-doped Ni/ $\gamma$ -Al<sub>2</sub>O<sub>3</sub> occurs with similar activation energies (80 kJ/mol), with slightly higher reaction order for hydrogen and lower reaction order for CO<sub>2</sub> than those observed for undoped Ni/ $\gamma$ -Al<sub>2</sub>O<sub>3</sub>. Lanthanum acts as a promoter because of the stronger basicity of the lanthana-alumina support allowing stronger adsorption of CO<sub>2</sub> as surface carbonates that can be act as "reactant reservoirs". The Ni/La-alumina catalysts studied here appear to be competitive with Ru/alumina catalysts for the selective CO<sub>2</sub> methanation at low temperature and atmospheric pressure.

## 1. Introduction

The hydrogenation of CO<sub>2</sub> to methane is a possible way to reuse captured CO<sub>2</sub>, thus reducing the emission of greenhouse gases by recycling carbon dioxide [1,2]. The use of hydrogen produced by water electrolysis using photovoltaic electricity production, or in any case the use of “renewable” hydrogen allows one to realize the “Power-to-Gas” (PtG) technology in a sustainable way [3,4]. The methane product, sometimes denoted as Synthetic or Substitute Natural Gas (SNG) [5], can be used as a green fuel and injected into existing natural gas pipeline networks. Through CO<sub>2</sub> methanation, “hydromethane”, a H<sub>2</sub>-CH<sub>4</sub> mixture, a potentially interesting fuel for automotive purposes [6], can be synthesized.

CO produced by the reverse water gas shift reaction (r-WGS) is an unwanted by-product from CO<sub>2</sub> methanation. Taking into account that methanation is an exothermic equilibrium reaction, catalysts for an efficient process must be active at low temperature, very selective and stable in practical conditions. Most of transition metals (such as nickel, cobalt and iron), and platinum group metals are active for both CO and CO<sub>2</sub> methanation reaction. However, the choice, for both CO<sub>2</sub> and CO methanation catalysts, is usually restricted to ruthenium and nickel. Ruthenium is more active, especially at low temperatures, and very selective to CH<sub>4</sub> starting from CO<sub>2</sub> [7,8,9]. Nickel is usually less active than Ruthenium, but can also give rise to high selectivities to CH<sub>4</sub>, depending on nickel loading [10]. Moreover, nickel is much cheaper than Ru, allowing one to use much higher metal loadings. As for the supports,  $\gamma$ -Al<sub>2</sub>O<sub>3</sub> is a widely produced and used material and support [11,12], with high dispersion properties for metals, usually giving rise to active and stable metal hydrogenation catalysts [13,14]. In fact, commercial catalysts for the already well-established CO methanation process in the purification of hydrogen (thus for low concentration CO<sub>x</sub> feeds) are based on either 0.3% Ru/ $\gamma$ -Al<sub>2</sub>O<sub>3</sub> (low temperature catalysts) or ~ 20% Ni/ $\gamma$ -Al<sub>2</sub>O<sub>3</sub> (high temperature catalysts) [15]. However, catalysts for SNG production, thus using concentrated feeds, may work at high temperatures. The use of a 22% Ni catalyst on a stabilized support, with a surface area decreasing from 50 m<sup>2</sup>/g (fresh) to 30 m<sup>2</sup>/g (used) has been reported [16]. In spite of the higher activity of Ru catalysts, according to Fechet and Vedin [17], “Ni/Al<sub>2</sub>O<sub>3</sub> is the best known catalyst for

industrial CO<sub>2</sub> methanation applications worldwide and it has been commercialized by Evonik, Johnson Matthey, Topsøe, and Clariant-Süd Chemie”.

To improve the CO<sub>2</sub> methanation process efficiency, a possible way is to improve the cheap Ni/ $\gamma$ -Al<sub>2</sub>O<sub>3</sub> catalysts, by tailoring optimal Ni particle size [18] and loading [10], thus increasing low temperature activity and CH<sub>4</sub> selectivity, as well as by stabilizing it structurally. We previously found that Lanthanum doping improves the properties of Ni/ $\gamma$ -Al<sub>2</sub>O<sub>3</sub> catalysts for steam reforming reactions [19]. Lanthanum is also reported to be fundamental in most of perovskite cathodes in Solid Oxide Fuel Cells [20] (i.e. LSM, LSCF etc.). On the other hand, lanthanum is reported to be a relevant additive to alumina in catalyst formulations: it improves alumina properties by increasing its mechanical strength [21] and stabilizing spinel-type alumina with respect to sintering and loss of surface area [22]. Additionally, it has been reported that lanthana can be used as precursor of sulfur-tolerant catalysts, being converted in situ to lanthanum oxysulfide (La<sub>2</sub>O<sub>2</sub>S) [23].

In previous papers we reported on the methanation activity of different Ni/Al<sub>2</sub>O<sub>3</sub> catalysts [10,24], as well as on the preparation and characterization of La<sub>2</sub>O<sub>3</sub>-Al<sub>2</sub>O<sub>3</sub> catalytic materials [25,26]. In the present paper we report on ways to improve the catalytic properties of a home-made 13.6 wt.% Ni/ $\gamma$ -Al<sub>2</sub>O<sub>3</sub> catalyst by modifying the alumina support with Lanthanum.

## 2. Experimental

### 2.1 Materials preparation

The catalysts were prepared using Puralox 200 Sba ( $\gamma$ -Al<sub>2</sub>O<sub>3</sub>, 200 m<sup>2</sup>/g) from Sasol previously calcined at 1023 K for 5 h as bare support. The catalytic materials, summarized in Table 1, were prepared through incipient wetness impregnation using La(NO<sub>3</sub>)<sub>3</sub>·xH<sub>2</sub>O (x~4) and Ni(NO<sub>3</sub>)<sub>2</sub>·6H<sub>2</sub>O (from Alfa Aesar and Sigma Aldrich, respectively) aqueous solutions. The theoretical amounts of La and Ni to obtain the designed % oxide on alumina (measured as  $100 \cdot g_{MO} / 100g_{cat}$  where MO is La<sub>2</sub>O<sub>3</sub> or NiO and cat is the total catalyst weight). Different La<sub>2</sub>O<sub>3</sub> contents in catalyst formulation (xLA, with x= 4, 14 and 37 wt.%) were achieved by dissolving the precursor salts in a volume of deionised water, in the way that the total liquid volume was equal to the pore volume of the material. A step of drying at 353 K in vacuum was undertaken for 15 h and calcination in air at 1023 K for 5 h with a

temperature ramping of 2 K/min was performed. The Ni/xLA catalyst was prepared using xLA as the support, thus the first impregnation was with La and the second with Ni precursors with an intermediate calcination of the support with the same procedure applied for the whole catalysts and reported above.

For the catalytic experiments and characterization, the catalysts were reduced in situ with a 20 mol% H<sub>2</sub>-80 mol% N<sub>2</sub> mixture and a total flow rate of 70 NmL/min. The heating rate was fixed at 25 K/min to 1023 K, then held for 30 min at that temperature. The catalysts were cooled to r.t. (room temperature) in the same atmosphere to avoid oxidation and kept in a pure nitrogen stream.

## 2.2 Materials characterization

Surface area measurements were performed in a Micromeritics Autochem 2920 with a single point measurement. The samples were pretreated in He at 523 K in order to desorb or decompose potentially adsorbed surface species.

X-Ray diffraction patterns were recorded using Cu K $\alpha$  radiation ( $\lambda=0.15406$  nm). XRD analysis of the fresh catalysts was performed on a Rigaku Smartlab Cu-source powder diffractometer. Cu K $\alpha$  radiation was used with a power setting of 45kV and 200mA with a scan rate of 2 $^\circ$ /min and a step size of 0.02 $^\circ$ . The patterns of the reduced samples were obtained using a vertical powder diffractometer X'Pert. Diffractograms were collected in the 15 – 100 $^\circ$  2 $\theta$  range with a step size of 0.02 $^\circ$  and a counting time for each step of at least 15 s. Powder patterns were indexed by comparing experimental results to the data reported in the Pearson's Crystal Data database [27].

Temperature Programmed Reduction with H<sub>2</sub> (H<sub>2</sub>-TPR) was used to identify and evaluate the reducibility of the various nickel species present on the alumina-supported catalysts. In a typical H<sub>2</sub>-TPR test, the as-calcined catalyst was reduced by a 10% H<sub>2</sub>/Ar gas mixture, while the temperature was increased from RT to 1173K at a rate of 15 K/min. In table 1, the mol<sub>H<sub>2</sub></sub>/mol<sub>Ni</sub> hydrogen consumption data during TPR are reported.

FT-IR spectra were registered with a Nexus Thermo Fisher instrument with 100 scans and spectra resolution of 2 cm<sup>-1</sup>. KBr pressed disks were used for skeletal characterization with a 1 wt.% catalyst and a disk total weight of 1.00 g. Pure powder pressed disks were used for surface characterization. The disks were previously activated by outgassing at 773 K

for 1 h. After activation, 50 Torr of CO<sub>2</sub> (SIAD, 99.99% grade) was introduced into the cell. After 10 min, brief outgassing at r.t. was realized and IR spectra recorded.

X-ray photoelectron spectroscopy (XPS) was conducted by using the Thermo Scientific monochromatic Al K-alpha line (1.4866 keV) as the excitation source. Binding energies were measured on a multi-channel detector with pass energy of 50 eV and energy step of 0.05 eV for high-resolution scans and 0.5 eV for survey scans. Spectral regions are Ni2p, Al2p and La3d. All the spectra were referenced to the elemental carbon at binding energy (BE) of 284.8 eV. Quantification of surface components was based on the peak fitting and normalization of Ni (2p 3/2), La (3d 5/2), and Al (2p) primary peaks.

Microscopic analyses were performed on a SEM ZEISS SUPRA 40 VP microscope, equipped with a field emission gun. This instrument is equipped with a high sensitivity "InLens" secondary electron detector, a solid state detector for backscattered electrons (BSE) and with an EDX microanalysis OXFORD "INCA Energie 450x3" for chemical analysis. Sample powders were directly mounted on a high purity conductive double sided adhesive carbon tabs, and the specimen so obtained was then imaged.

### *2.3 Catalytic experiments*

A tubular silica glass flow reactor, containing a fixed bed with 88.2 mg of catalyst mixed with 700 mg of silica glass particles 0.25–0.21 mm (corresponding to 60-70 mesh sieved) was used in steady-state catalytic experiments. CO<sub>2</sub> hydrogenation experiments were conducted with the following feed gas: 6% CO<sub>2</sub>, 30% H<sub>2</sub> and N<sub>2</sub> balance, used as carrier gas. The gas hourly space velocity GHSV was equal to 55000 h<sup>-1</sup>. In order to follow any hysteresis, activation or deactivation effects, experiments were performed both in ascending and descending reaction temperature (523 K, 573 K, 623 K, 673 K, 723 K, 773K and reverse).

Online products analysis was performed using a Nicolet 6700 FT-IR instrument. Frequencies, where CO<sub>2</sub>, CH<sub>4</sub> and CO molecules absorb weakly, were used (2293 cm<sup>-1</sup> for CO<sub>2</sub>, 2170 cm<sup>-1</sup> for CO, 1333 cm<sup>-1</sup> for CH<sub>4</sub>, after subtraction of baseline) with previous calibration using gas mixtures with known concentrations, in order to have quantitative results. Produced water was condensed upstream of the IR cell. From the inlet and outlet concentrations calculated from the absorbances of CO, CO<sub>2</sub>, CH<sub>4</sub> and the measured inlet and outlet total flows (which allow to take into account the variation of the number of moles

during the reaction), CO<sub>2</sub> conversion ( $X_{CO_2}$ ), selectivities and yields to products,  $S_i$  and  $Y_i$ , were calculated [28]. They are defined as:

$$X_{CO_2} = \frac{F_{CO_2 in} - F_{CO_2 out}}{F_{CO_2 in}} \quad (4)$$

$$S_i = \frac{F_i}{F_{CO_2 in} - F_{CO_2 out}} \quad (5)$$

$$Y_i = \frac{F_i}{F_{CO_2 in}} \quad (6)$$

where  $F_i$  is the molar flow rate of  $i$  (i.e. CO and CH<sub>4</sub>), while  $F_{CO_2}$  is the molar flow rate of CO<sub>2</sub>, all expressed in mol/min.

In order to investigate kinetic aspects, the catalysts were pretreated as previously reported. In this case, 88.2 mg of catalysts were diluted in 350 mg of silica glass. To study the CO<sub>2</sub> reaction order, CO<sub>2</sub> partial pressure was varied between 0.02 atm and 0.07 atm while maintaining constant hydrogen partial pressure ( $p_{H_2} = 0.30$  atm). The reaction temperatures were fixed at 493 K and 523 K for Nickel based catalysts, where the hypothesis of a differential reactor can be applied (CO<sub>2</sub> conversion in 3-15% range). The same procedure and hypothesis were made to study the reaction order with respect to H<sub>2</sub> concentration, where  $p_{H_2}$  was varied from 0.03 atm to 0.28 atm at constant  $p_{CO_2}$  (0.07 atm). At low temperature, an estimation of the apparent activation energy of CO<sub>2</sub> methanation was done, using the conversion values obtained under kinetic control at 493 K, 523 K and 573 K, thus deriving Arrhenius- type plots [29].

It should be noted that we did not observe any coke formation in our experiments, each performed over 8 h. Carbon balance was 100%  $\pm$  1% in our calculations and no evidence of coke was obtained from the catalyst weight measurements nor from FE-SEM studies of Ni- catalysts. Moreover, the amount of liquid water formed during reaction was measured at the end of each experiment, allowing to evaluate the goodness of our tests and as a further check of total mass balance.

### 3. Results

#### 3.1 Characterization of the fresh catalyst

### 3.1.1 Surface area measurements.

The surface area of the pure alumina support, calcined at 1023 K for 5 h, is 170 m<sup>2</sup>/g. The sequence of impregnation of lanthanum and nickel reduces the surface area, to nearly 150 m<sup>2</sup>/g for NiØLA and Ni4LA, down to 130 m<sup>2</sup>/g and 100 m<sup>2</sup>/g for Ni14LA and Ni37LA, respectively.

### 3.1.2 XRD

In Figure 1, the XRD patterns of the as prepared samples under study are reported together with the diffractograms of the corresponding supports. The diffraction patterns of NiØLA, Ni4LA and Ni14LA show, with respect to  $\gamma$ -Al<sub>2</sub>O<sub>3</sub> (ØLA), an intensification and a shift toward smaller 2 $\theta$  of the 400 and 440 spinel peaks and, in particular, to those assigned to the 311 peak, with almost complete disappearance of the 222 one. The resulting diffraction pattern is similar to that observed for NiAl<sub>2</sub>O<sub>4</sub> inverted spinel [30] even if the composition is still cationically deficient (Ni<sub>0.26</sub>Al<sub>2</sub>O<sub>3.26</sub> in line with the determined EDX composition Ni<sub>0.36</sub>Al<sub>2</sub>O<sub>3.36</sub>) with respect to the spinel composition, although less deficient than  $\gamma$ -Al<sub>2</sub>O<sub>3</sub>. This is in line with previous studies that showed that XRD patterns of both cationically deficient and stoichiometric NiAl<sub>2</sub>O<sub>4</sub> are very similar [30,31]. As already reported, a strong interaction of surface Ni with alumina occurs with the formation of surface or subsurface Ni aluminate and this is evident by observing the shift toward low 2 $\theta$  values of the 440 peak that corresponds to a slight expansion of the cubic cell volume [32]. The presence of lanthanum does not modify the diffractogram in these cases and a constant 2 $\theta$  shift of the 440 peak is observed for the three samples. The picture for the samples NiØLA, Ni4LA and Ni14LA suggests that Ni spreads and strongly interacts with the alumina surface while lanthanum disperses over the surface without a significant perturbation of the bulk.

A different situation is observed for the Ni37LA catalyst. In this case, several different phases are found together with the spinel. In fact, the presence of La(OH)<sub>3</sub> and a rhombohedral perovskite LaAlO<sub>3</sub>, phases are observed, as found in the corresponding La<sub>2</sub>O<sub>3</sub>-Al<sub>2</sub>O<sub>3</sub> "support" [25]. The presence of NiO (bunsenite, JCPDS table 04-0835) is clearly observed only for the Ni37LA sample, while it is not present in other samples whose Ni loading is the same [33]. This might be due to the significant reduction of the surface area of the La-rich support and/or to its different composition, resulting in a lower interaction of Ni with the surface favouring the oxide formation.

In Figure 2, the diffraction patterns of the reduced catalysts are reported. As expected, reduction of Ni $\emptyset$ LA, Ni4LA and Ni14LA produces cubic metallic Nickel with a reappearance of the characteristic 222 peak typical of  $\gamma$ -Al $_2$ O $_3$ , and a shift of  $\gamma$ -Al $_2$ O $_3$  peaks to the characteristic listed structure peaks [13, 27]. This indicates that, upon reduction, the surface or sub-surface aluminate phase produces less dispersed nickel as Ni nanoparticles.

For Ni37LA, the disappearance of the peak corresponding to NiO is observed with the appearance of cubic metallic nickel. For this sample, an increased crystallinity is observed after reduction with a clear appearance of the peaks assigned to La(OH) $_3$ . For the metallic Ni phase, an evaluation of crystallite size through the Scherrer formula, using the (2,0,0) crystal plane family, determined particle diameters of 7 nm, 8 nm, 10 and 15 nm in the four samples, at increasing, from 0 to 37 wt. %, La $_2$ O $_3$  loading, with a linear trend. To calculate crystallite dimensions, data have been previously treated with a smooth function, and then the line profile peaks have been fitted with a pseudo-Voigt function.

### 3.1.3 Skeletal IR and UV-vis spectroscopic characterization of unreduced catalysts.

In Figure 3, the infrared skeletal spectra of the materials are reported. The spectra of Ni-containing samples markedly differ from the spectra of the Ni-free “supports” because of the presence of a pronounced component at 723 cm $^{-1}$ , as well as to a slight shift downwards of the main band from near 545 cm $^{-1}$  to 508 cm $^{-1}$ . This confirms the results obtained by XRD showing the features of spinel NiAl $_2$ O $_4$  or of cationically deficient Ni $_x$ Al $_2$ O $_{3+x}$  spinels, which are very similar each other [30]. A different situation is found for Ni37LA where the feature at 429 cm $^{-1}$  is associated to the presence of bulk NiO [34,35,36,37] which masks the features of other phases such as LaAlO $_3$  [19,38]. The presence of lanthanum species is confirmed by the fingerprint of carbonate features (1400 and 1491 cm $^{-1}$ ) which can be associated either with surface or bulk lanthanum carbonates [39,40]. It is noted that the carbonate band intensities increase as the La- loading increases.

In Figure 4, the diffuse reflectance UV-visible spectra (DR-UV-vis-NIR) of the as prepared catalysts are reported. Ni $\emptyset$ LA, Ni4LA, Ni14LA spectra show absorption in the visible region, characterized by a split band at 601 and 633 nm, which is attributed to the  $^3A_{2g} \rightarrow ^3T_{1g}$  d–d transition of Ni $^{2+}$ , split for the presence of the weaker  $^3A_{2g} \rightarrow ^1E_g$ , whose position and shape are typical of Ni $^{2+}$  dispersed on alumina [31,41] in an environment

similar to that of NiAl<sub>2</sub>O<sub>4</sub> spinel. Moreover, the clear absence of the feature at 718 nm indicates that NiO species are not present in any of the three catalysts [31]. By looking at the NIR region, a broad band is observed near 1048 nm that is assigned to  $\nu_1$  ( ${}^3A_{2g} \rightarrow {}^3T_{2g}$ ) transition of Ni<sup>2+</sup> in octahedral surroundings in a position similar to the one reported for low loading Ni catalysts, i.e. NiAl<sub>2</sub>O<sub>4</sub> [42] and Ni highly dispersed on alumina [32,33].

Indeed, the spectra of NiØLA, Ni4LA and Ni14LA look qualitatively similar in the visible region, although the addition of lanthanum seems to slightly increase the background absorption. At lower wavenumbers, in the UV region, the addition of Lanthanum seems to cause the formation of a shoulder centered around 310 nm, absent in the case of the NiØLA sample, at the high wavenumber side of the absorbance increase due to the a O<sup>2-</sup> (2p) → Ni<sup>2+</sup> (3d) charge transfer transition. This shoulder, located at lower energy than the corresponding transition of isolated Ni<sup>2+</sup> on alumina, can be associated to Ni<sup>2+</sup> species interacting with other Ni<sup>2+</sup> or with La<sup>3+</sup> species.

In agreement with the XRD results, a different situation is observed for Ni37LA. This sample is absorbing a great part of the radiation, inhibiting the possibility to observe characteristic absorption in the visible range. This might be due to the strong absorption of the visible light by LaNiO<sub>3</sub> perovskite [43]. Additionally, the sample shows a cut off near 350 nm due to the appearance of the strong O<sup>2-</sup> (2p) → Ni<sup>2+</sup> (3d) charge transfer transition of bulk NiO, in agreement with XRD and H<sub>2</sub>-TPR data.

These spectroscopic data confirm that, even in the presence of significant amounts of lanthanum, nickel strongly interacts with alumina. Only at the highest La loading, the situation changes, with the formation of lanthanum rich phases.

#### 3.1.4 XPS analysis of unreduced catalysts.

In Fig. 5, the XP spectra are reported in the Al(2p), Ni(3p) and La(3d 5/2) regions. The Al(2p) spectra of NiØLA, Ni4LA and Ni14LA show a significant shift of the main peak from 74.2 eV, value reported for  $\gamma$ -Al<sub>2</sub>O<sub>3</sub> [44,45], down to 73.9 eV for Ni4LA and Ni14LA and further shifting to 73.5 for Ni37LA. The shift of the XP peak to lower binding energy is interpreted as due to a decreased ionicity of the Al-O bond [46] or to a higher density of the phase [47]. In any case the trend, i.e. the shift increasing with increasing Ni loading, seem to further indicate a strong interaction of Ni with surface Al ions. In the same region, an additional component appears at 68.9 eV for NiØLA, shifting to 68.2 eV and 68.0 for

Ni4LA and Ni14LA samples respectively, which is due to Ni 3p core level spectra of Ni<sup>2+</sup> species [48,49]. A split of the components is observed for Ni37LA where signals at 69 and 67 eV are present showing that an additional Ni-containing species is formed, which can be identified as LaNiO<sub>3</sub> phase [50] or LiAl<sub>1-x</sub>Ni<sub>1-x</sub>O<sub>3</sub> solid solution.

The XP spectrum of NixLA samples in the 830-845 eV region (Fig. 5) is due to lanthanum 3d<sub>5/2</sub> transition. The peak positions we found for the three La-containing catalysts are close to 835.0 eV and 838.5 eV, at slightly higher energies than those reported for bulk La(OH)<sub>3</sub> [51], La<sub>2</sub>O<sub>3</sub> [51,52,53], LaAlO<sub>3</sub> [51,53], and for a number of La hexaaluminates [54,55,56] but in good agreement with our previous results [19].

The XP spectrum of the NiA sample, in the Ni 2p<sub>3/2</sub> region (830-865 eV) (Fig. 6), shows two main peaks at 856.1 and 862.3 eV which compare quite well with the spectra reported of NiAl<sub>2</sub>O<sub>4</sub>, Ni/Al<sub>2</sub>O<sub>3</sub> samples [57, 58] and LaNiAl<sub>11</sub>O<sub>19</sub> [55,56]. They can be assigned to a Ni<sup>2+</sup> main component and its satellite line ( $\approx$  862 eV). For La and Ni containing samples, the XP spectra in the La 3d<sub>3/2</sub> and Ni 2p<sub>3/2</sub> region (830-860 eV) are partially overlapped (Fig. 6). The doublet due to La 3d<sub>3/2</sub> ( $\approx$  852 and 855.5 eV) increases in intensity with increasing Lanthanum loading (as expected), while the Ni 2p<sub>3/2</sub> doublet shifts slightly and progressively to lower energies down to about 855 and 861 eV. This behavior confirms some interaction occurs between Ni<sup>2+</sup> and La<sup>3+</sup> centers. The low binding energies of Ni2p<sub>3/2</sub> observed in Ni37LA can be assigned to the presence of NiO with the characteristic peak at 853.7 eV [31]. On Ni37LA, an additional peak is clearly observable at 866 eV and it is assignable to the plasmon component of La [59], not detectable for low-loaded lanthanum catalysts. By looking at the surface elemental composition, coming from XP spectra of the as prepared catalysts (Table 2), it is possible to detect that the addition of lanthanum on Ni4LA is at the expense of surface Al, not of nickel. This indicates that, in the case of this sample, the addition of lanthanum allows to nearly complete the surface “monolayer” of supported species on the alumina surface. In the case of Ni14LA also the surface Ni is slightly reduced but the Ni-alumina interaction is still nearly intact. A completely different situation is found for the Ni37LA sample where, in agreement with XRD data, alumina reacts with lanthanum and nickel oxide species.

### 3.1.5. IR surface characterization of unreduced catalysts.

In Fig. 7, left, the IR spectra of the surface hydroxyl groups of the samples are compared. It is evident that the addition of lanthanum as well as of nickel causes the decrease of the

intensity of the OH stretching bands of the surface hydroxyl groups. This is in line with a progressive coverage of the alumina surface. In Figure 7 right, the spectra of carbonate species resulting from CO<sub>2</sub> adsorption and short outgassing at r.t. are reported. The spectrum observed on bare alumina is due to two types of hydrogencarbonate species ( $\nu_{\text{as}} \text{COO}$  at 1644 cm<sup>-1</sup>,  $\nu_{\text{sym}} \text{COO}$  split at 1484 and 1442 cm<sup>-1</sup>,  $\delta\text{OH}$  at 1236 cm<sup>-1</sup>), as reported many times [25,26]. The spectra of both 4LA and Ni4LA show the bands of one hydrogencarbonate type only, indicating that the deposition of Lanthanum is “selective” and “poisons” the more active AlOH and Al<sup>3+</sup>-O<sup>2-</sup> acido-basic couples of alumina, as discussed elsewhere [19]. The addition of Ni to 4LA causes a slight decrease of the above bands and the appearance of broader bands near 1540 and around 1400 cm<sup>-1</sup>, likely due to bidentate (bridging or chelating) species. In the case of 14LA and Ni14LA samples, the bands of hydrogencarbonate species are still present but much lowered in intensity; in particular, a weak feature at 1229 cm<sup>-1</sup> is still evident. This suggests that a small fraction of alumina is still exposed at the surface. However, additionally, strong bands due to carbonate species are also observed. Two couples are observed, i.e. at 1610, 1380 cm<sup>-1</sup> and at 1540, 1435 cm<sup>-1</sup>. Outgassing at r.t. (data not reported) shows that the former couple is associated with a more weakly adsorbed species while the latter is associated with a stable species. The former couple decreases in intensity by further adsorbing Nickel, while the latter does not seem to be modified by nickel addition.

The above data suggest that in the case of Ni4LA the addition of Nickel mostly shifts a large part of lanthanum from the strongest alumina sites (where they do not form basic sites) to weaker ones, generating La-O basic sites adsorbing CO<sub>2</sub> as carbonates. On 14LA, a large part of lanthanum forms basic sites where CO<sub>2</sub> is adsorbed as carbonate species. Addition of Nickel on 14LA producing Ni14LA causes the decrease of the number of the La-O sites producing carbonates species not stable at the surface. This suggests that Ni displaces lanthanum from alumina sites where it produces weak basic sites, causing its agglomeration.

### 3.1.5 H<sub>2</sub>-Temperature Programmed Reduction (H<sub>2</sub>-TPR).

H<sub>2</sub>-TPR data are reported in Fig.8 and the obtained H<sub>2</sub> consumptions are included in Table 1. In all cases, with the exception of Ni37LA, only one peak is present and it is centered at 1073 K corresponding to a complete reduction of well dispersed Ni oxidized species to the metallic state. A careful look to H<sub>2</sub>/Ni ratio (Table 2) points out a slight apparent excess of

hydrogen consumption with respect to the expected 1:1 stoichiometry (assuming Ni as Ni<sup>2+</sup>), that might be due to possibly adsorbed (on Ni) and spillover hydrogen [60]. For Ni $\emptyset$ LA, Ni<sub>4</sub>LA and Ni<sub>14</sub>LA, the reduction onset is observed near 740 K. The high reduction temperature identified in these samples indicates the presence of poorly reducible Ni species, strongly interacting with the support, in accordance with the XRD and UV-vis findings. This is typical of Ni/Al<sub>2</sub>O<sub>3</sub> systems [34]. Only in the case of Ni<sub>37</sub>LA, the quite complex peak associated with reduction of free NiO, typically centered at 500-800 K, is observed even if it could be partially overlapped with the one arising from methane production by reduction of surface carbonate species [61].

### 3.1.6 FE-SEM of reduced catalysts.

The reduced catalysts were characterized by means of FE-SEM equipped with EDX microanalysis. Catalyst composition was determined by EDX at very low magnification and the results are summarized in Table 2. Ni, La and Al loadings, determined experimentally, are in line with those designed and expected for the prereduced catalysts, although Al compositions are usually underestimated respect to nominal bulk composition values, especially at increasing La<sub>2</sub>O<sub>3</sub> loading.

The images obtained with backscattered electrons (BSE) show that the heavier elements, Ni and La, are homogeneously distributed in the case of unreduced Ni $\emptyset$ LA, Ni<sub>4</sub>LA and Ni<sub>14</sub>LA (pictures are not shown here, because there is no contrast in the images). In contrast, as depicted in Figure 9, the images of prereduced catalysts show clearly small bright particles of metallic Ni nanoparticles with a narrow particle size distribution and an average diameter lower than 10 nm, whose size agrees with that calculated from the XRD peaks using the Scherrer method. Lanthanum also is homogeneously distributed on catalysts surface; in fact, particles morphology and dimensions do not change passing from Ni $\emptyset$ LA to Ni<sub>14</sub>LA. A completely different situation is observed for the sample with the highest La<sub>2</sub>O<sub>3</sub> loading, i.e. Ni<sub>37</sub>LA, where the catalyst morphology is completely changed from a globular-like structure to a sponge like one (Figure 9, secondary electron micrograph (SE) and in the inset BSE one). In this case, a La-rich globular phase, with an average diameter of 10-30 nm, covered quite completely the sample surface. For this reason, the EDX analyses of this sample quantify a lower Al content than the expected.

## 3.2 Catalytic activity studies

### 3.2.1 Catalytic activity in CO<sub>2</sub> methanation

In Figure 10, the catalytic activity in terms of CH<sub>4</sub> and CO yields for all the investigated catalysts is reported. In the same figure, the values corresponding to thermodynamic equilibrium are as well included. No other C-containing products are observed. The thermodynamic equilibrium has been evaluated in the applied experimental conditions by using a Gibbs reactor and Soave – Redlich – Kwong equation of state. It has been verified that, in our conditions, no carbon deposition is expected by thermodynamics. At temperatures lower than 623 K, the observed CO<sub>2</sub> conversion and CH<sub>4</sub> yields are much lower than that allowed by thermodynamics, and significant differences in between the investigated catalysts can be observed. This agrees with a kinetically controlled regime. Instead, above 673 K the regime is roughly thermodynamically- controlled in all cases. At the same temperature in increasing and decreasing temperature experiments, CO<sub>2</sub> conversion is nearly constant for NiØLA, Ni4LA and Ni14LA, thus excluding detectable deactivation and/or conditioning effects. In the kinetically-controlled regime the activity follows the order: Ni14LA >Ni4LA ≈ Ni37LA >NiA suggesting that lanthanum addition is beneficial for CO<sub>2</sub> hydrogenation activity, with the best composition of near 14 wt.% La<sub>2</sub>O<sub>3</sub>. Ni14LA is also the catalyst that reaches thermodynamic equilibrium at the lowest temperature (673 K). Methane is found as the main product at low temperature, where the reaction is under kinetic control, with a selectivity approaching 100% at T ≤ 623 K in particular on the most active Ni14LA catalyst, where the methane yield is around 90 % at 623K (with undetectable CO amount). Thus, in these conditions, only the Sabatier reaction (reaction 1) is observed



CO production is nearly zero at low temperatures over the La-containing catalyst, but is non-negligible over the La-free catalyst. At higher temperatures (> 700 K), where the reaction is under thermodynamic control CO is also detected as a by-product in amounts approaching those expected by thermodynamics over all catalysts.

It must be considered that the reverse water gas shift reaction (reaction 2).



producing CO from CO<sub>2</sub> hydrogenation, is an endothermic equilibrium reaction, that, however, may allow significant CO<sub>2</sub> conversion to CO in the range 523-623 K. However, both CO and CO<sub>2</sub> methanation are favored in the same low temperature range, and this is the reason why CO production from CO<sub>2</sub> hydrogenation can be very selective to CH<sub>4</sub> in the presence of very active methanation catalysts. Thus, it is evident that lanthanum addition certainly strongly enhances the methanation rate with respect to La-free catalyst.

### 3.2.2 Evaluation of reaction order and apparent activation energies

In Figure 11, the determination of reaction orders for CO<sub>2</sub> and H<sub>2</sub> in the condition of a differential reactor with CO<sub>2</sub> conversions generally lower than 13% and where approach to equilibrium can be neglected. The rate data have been fitted with a simple power law expression [62] in the form:

$$r_{CH_4} = k * p_{H_2}^\alpha p_{CO_2}^\beta$$

and the determined reaction orders are summarized in Table 3. This expression is considered an excellent model in differential studies [63] even though not suitable in the entire range of operation conditions. As a function of the lanthanum loading the reaction order of H<sub>2</sub> ( $\alpha$ ) slightly increases while for  $\beta$ , reaction order of CO<sub>2</sub>, a progressive decrease from 0.20 to 0.14 is observed, suggesting a stronger interaction of CO<sub>2</sub> when lanthanum is introduced in the catalyst formulation, likely due to a stronger adsorption of CO<sub>2</sub> on the catalyst surface. In the case of the most active catalyst, Ni14LA, CO<sub>2</sub> methanation kinetics was investigated at 493 K. The reaction orders, evaluated in this case, are different from those evaluated at 523 K ( $\alpha=0.28$  and  $\beta=0.14$ ), suggesting that a non-negligible temperature dependence is present for both reaction orders. The behavior is similar to the one previously reported by Weatherbee and Bartolomew [62] for low-loading Ni/SiO<sub>2</sub> catalysts. In particular, also in this case, the CO<sub>2</sub> order decreases with a temperature increase, while H<sub>2</sub> reaction order increases with a temperature increase.

In Figure 12, the Arrhenius plot for the tested catalysts is reported. In all cases, the apparent activation energies are in the range of 70-85 kJ/mol, proper of a true kinetic regime with a negligible contribution due to diffusional limitations. Those values are in agreement with apparent activation energies reported on Ni/Al<sub>2</sub>O<sub>3</sub> ( $E_a=80$  kJ/mol) [10,24] and more realistic than values reported on a recent paper of Ni modified lanthanum hydrotalcite catalysts where value of 1.4-1.6 kJ/mol were obtained, typical of a diffusion limited regime [64].

## 4. Discussion

The data reported here show that all Ni<sub>x</sub>LA catalysts are active for the CO<sub>2</sub> hydrogenation at atmospheric pressure and in excess hydrogen conditions. The La-free catalyst tested here is more active than a 20% Ni/ $\gamma$ -Al<sub>2</sub>O<sub>3</sub> commercial catalyst tested in the same conditions as reported in our previous work [24] despite the lower nickel content in our

preparation. However, it must be taken into account that while our material was prepared by incipient wetness impregnation on the support powder, industrial catalysts preparation can be made by impregnation of support extrudates. Thus, in the industrial case, Ni loading may be higher at the surface of the pellet and lower in the center of it, thus the nominal Ni loading is the average of highly loaded particles and almost pure alumina.

A slight reduction of the activation energy is observed for our catalyst with respect to commercial Ni- $\gamma$ -Al<sub>2</sub>O<sub>3</sub> catalyst further confirming the catalytic activity data. Similarly, small differences are observed in the estimated reaction orders where a slight increase is observed for both the H<sub>2</sub> and CO<sub>2</sub> reaction orders 0.41 for H<sub>2</sub> and 0.20 for CO<sub>2</sub> with respect to the ones determined for commercial Ni/Al<sub>2</sub>O<sub>3</sub> catalyst [24]. Our values are also higher than those reported for coprecipitated Ni/Al<sub>2</sub>O<sub>3</sub> catalysts [63].

Moderate lanthanum addition (4 and 14 wt.% La<sub>2</sub>O<sub>3</sub>) does not modify the Ni reduction profile. This suggests that, still, a strong interaction between metal and support is present as suggested also from the UV-vis data where the typical components of Ni<sup>2+</sup> species were found. Moreover, the stable high surface area, compared to the support, confirms the beneficial effect of lanthanum addition in increasing the thermal stability of the alumina support. This feature is important due to the high exothermicity of the methanation reaction. In the case of all Ni<sub>x</sub>LA catalysts, prereduction gives rise to mainly metallic nickel particles with characteristic diameters lower than 10 nm, comparable to those reported for prereduced Ni<sub>16</sub> on a Si stabilized alumina support [10] that were found to be extremely selective for methane with no CO coproduction.

Our data show that the introduction of Lanthanum in the catalyst formulation even at low loadings strongly increases the catalytic activity in the 500-630 K temperature region, with a simultaneous increase in methane selectivity to ~ 100%. These data roughly agree with the recent results reported by Rivero -Mendoza et al. [65] but disagree with those reported by Rahmani et al. [66] where deactivation was observed for 2%La<sub>2</sub>O<sub>3</sub>-Ni/Al<sub>2</sub>O<sub>3</sub> catalyst in CO<sub>2</sub> methanation. They are also in line with studies of CO methanation studies that reported an activation effect of lanthanum on Ni/Al<sub>2</sub>O<sub>3</sub> [67] as well as on Ni/Mg-Al<sub>2</sub>O<sub>3</sub> ex hydrotalcite catalysts [68]. The data also show a slight increase in the reaction order of CO<sub>2</sub>, which can be attributed to an increased basicity, hence an increased adsorption strength of CO<sub>2</sub>, on the support. This is in line with the data discussed by some of us years ago [69] and reported by recent authors for CO<sub>2</sub> methanation on alumina-supported metals

[8,9], suggesting that CO<sub>2</sub> adsorption takes primarily occurs on the alumina support. Additionally, a slight decrease is found of the reaction order of H<sub>2</sub> by addition of lanthanum, which may be in line with the easier hydrogenation of more strongly adsorbed CO<sub>2</sub>, or with some effect of lanthanum on nickel in making easier the activation of hydrogen, that certainly occurs on the metal.

Previous studies from our laboratory [25,26] have shown that the addition of lanthanum to alumina reduces the number of very active Al<sup>3+</sup>-O<sup>2-</sup> acido-basic surface sites and produces new basic sites probably of the La<sup>3+</sup>-O<sup>2-</sup> type [25]. IR data, visible spectroscopy data and Al (2p) XPS data show that, in the case of Ni4LA and Ni14LA, Ni strongly interacts with alumina surface producing a spinel-like surface layer as it does on bare alumina. This occurs by displacing pre-impregnated La-O species from the strongest alumina acido-basic sites to weaker ones, where their acidity is even stronger. However, both UV spectroscopy and Ni (2p 3/2) XPS data provide evidence of some interactions between La<sup>3+</sup> and Ni<sup>2+</sup> centers in the case of as prepared catalysts, that could result in some interaction also in the reduced catalysts. On the other hand, the Ni+La loading in Ni4LA is nearly the one needed to complete (theoretically) the monolayer coverage, while in the case of the Ni14LA sample this amount is (theoretically) by larger than that required for a monolayer, at least in the unreduced state. However, IR data of CO<sub>2</sub> adsorption suggest that, in both cases, a small fraction of alumina is still uncovered, thus the Ni species grow in 3-D, leaving some small alumina areas in between, in parallel to the partial recovery of the  $\gamma$ -Al<sub>2</sub>O<sub>3</sub> XRD pattern upon reduction. Additionally, nickel species seems to strongly interact with the alumina surface irrespective of the lanthanum loaded.

The addition of lanthana, resulting in the formation of basic sites, which adsorb CO<sub>2</sub> more strongly, could be beneficial for CO<sub>2</sub> methanation because of the stronger adsorption of CO<sub>2</sub> on the support. This can occur because the support can act as a CO<sub>2</sub> reservoir, by adsorbing it as carbonate species, allowing easier spillover of CO<sub>2</sub> from the support to the Ni particles where reaction takes place, or because surface carbonates are hydrogenated by spillover of hydrogen. In any case, a stronger basicity can explain a stronger adsorption of CO<sub>2</sub> and the (weak) trend to a lower reaction order with respect to CO<sub>2</sub>.

On the other hand, as suggested by XPS and UV spectra of the unreduced catalysts, the presence of lanthanum species may also influence Ni particle formation. Wierbizcki et al. [64] proposed that an electronic interaction may occur among La species and Ni particles. In our case, we cannot draw definitive conclusions on the basis of the data available up to

now. In any case, the decrease of the adsorption strength of hydrogen (as deduced by the increased reaction order with respect to hydrogen) and the increased methane selectivity are relevant, and may be due to increased hydrogenation activity.

It seems quite interesting that the catalytic activity of our Ni14LA catalyst is nearly the same or even slightly better than the activity of a commercial 3 wt.% Ru/Al<sub>2</sub>O<sub>3</sub> catalyst tested in the same conditions: as an example, methane yield is 66% at 573 K on 3 wt.% Ru/Al<sub>2</sub>O<sub>3</sub>, while nearly 72 % on Ni14LA. While Ru/alumina catalysts can also be improved by promoters, it seems that robust and cheap Ni/alumina catalysts could be competitive with the much more expensive Ru- based catalysts, thus preferable for low-temperature for CO<sub>2</sub> hydrogenation.

## 5. Conclusions

The following conclusion points are drawn from the findings of this work:

1. Lanthanum addition strongly increases the activity of Ni/ $\gamma$ -Al<sub>2</sub>O<sub>3</sub> for CO<sub>2</sub> methanation. In addition, selectivity to methane is increased up to nearly 100% at low temperatures, where the reaction is in the kinetic regime ( $T < 650\text{K}$ ).
2. The CO<sub>2</sub> methanation reaction on La-doped Ni/ $\gamma$ -Al<sub>2</sub>O<sub>3</sub> occurs with similar activation energies (80 kJ/mol), a slightly higher reaction order for hydrogen and a lower one for CO<sub>2</sub> than undoped Ni/ $\gamma$ -Al<sub>2</sub>O<sub>3</sub>.
3. Characterization data suggest that nickel oxide species interact with the alumina surface more strongly than lanthanum oxide. Thus, the impregnation of Ni species over lanthanum-alumina shifts lanthanum from the strongest acido-basic sites of the alumina surface (where they do not form basic sites) to weaker alumina sites (where they form stronger La-O basic sites).
4. It is proposed that lanthanum acts as a promoter because of the stronger basicity of the lanthana-alumina support allowing stronger adsorption of CO<sub>2</sub> as carbonates acting as reactant reservoirs, while activation of hydrogen on nickel is also slightly improved by the presence of La .
5. La-doped Ni/ $\gamma$ -Al<sub>2</sub>O<sub>3</sub> catalysts are competitive with Ru/alumina catalysts for the selective CO<sub>2</sub> methanation at low temperatures and atmospheric pressure.

## Acknowledgements

G.G. acknowledges University of Genova for the support to conduct research at Tufts University. Ioannis Valsamakis is gratefully acknowledged for his participation in catalyst preparation and characterization. G.G. and G.B. acknowledge Giulia Piazza for the experimental work on methanation reaction carried out during her bachelor thesis. M.F.-S., and C. W. acknowledge the financial support of the work at Tufts by the U.S. Department of Energy, Grant # DE-FG02-05ER15730.

## Figure captions

Figure 1. X-Ray diffraction patterns of as cast supports (xLA) and unreduced Ni-based catalysts (NixLA) together with the identification of crystalline phases [27].

Figure 2. X-Ray diffraction patterns of reduced NixLA catalysts and identification of the crystalline phases

Figure 3. Skeletal IR spectra of as cast supports xLA and unreduced NixLA catalysts.

Figure 4. DR-UV-vis spectra of NixLA catalysts (full lines) and NiO reference sample (dotted line)

Figure 5. (left) Al(2p) and Ni (3p) regions (80-64 eV) and (right) La (3d 5/2) region (845-830 eV).

Figure 6. XP spectra of NixLA catalyst in the Ni(2p 3/2) region (870-845 eV).

Figure 7. (right) IR spectra of xLA and NixLA in the OH region and (left) IR spectra of xLA and NixLA catalysts upon CO<sub>2</sub> adsorption.

Figure 8. H<sub>2</sub>-TPR profiles of the investigated NixLA catalysts.

Figure 9. FE-SEM micrographs acquired in BSE electrons for NixLA catalysts (x= 0, 4 and 14). In Ni<sub>37</sub>LA secondary electron images is reported and correspondingly the BSE image in the bright region is included in the inset.

Figure 10 Methane and CO yields obtained in CO<sub>2</sub> hydrogenation for prereduced NixLA catalysts (symbols) in the 523-773 K temperature region with the comparison of thermodynamic equilibrium values. Experiment conditions: 6% CO<sub>2</sub>, 30% H<sub>2</sub>, N<sub>2</sub> balance and a total flow rate of 80 Nml/min, atmospheric pressure.

Figure 11. (left) Methane production rate as a function of H<sub>2</sub> partial pressure in kinetic evaluations for NixLA catalysts and (right) Methane production rate as a function of CO<sub>2</sub> partial pressure.

Figure 12. Arrhenius plot for evaluation of apparent activation energies.

Table 1: Composition, surface area and hydrogen consumption data

	NiO wt%	La <sub>2</sub> O <sub>3</sub> wt%	BET Surface area	H <sub>2</sub> consumption
	W <sub>NiO</sub> /W <sub>cat</sub> [%]	W <sub>La2O3</sub> /W <sub>cat</sub> [%]	[m <sup>2</sup> /g]	[μmol/g]
NiA	16.7%	-	151	3159
Ni4LA	16.7%	4%	150	3142
Ni14A	16.7%	14%	131	3051
Ni37LA	16.7%	37%	100	2974

Table 2: Composition of reduced catalysts (design and EDX compositions) and on the as prepared catalysts (XPS composition).

	Design composition			EDX composition			XPS surface composition				H <sub>2</sub> /Ni
	Ni wt. %	La wt. %	Al wt. %	Ni wt. %	La wt. %	Al wt. %	Ni	La	Al	O	From TPR
	W <sub>Ni</sub> /W <sub>cat</sub> [%]	W <sub>La</sub> /W <sub>cat</sub> [%]	W <sub>Al</sub> /W <sub>cat</sub> [%]	W <sub>Ni</sub> /W <sub>cat</sub> [%]	W <sub>La</sub> /W <sub>cat</sub> [%]	W <sub>Al</sub> /W <sub>cat</sub> [%]	at. %	at. %	at. %	at. %	[-]
NiØLA	13.6%	-	45.7%	13.5%	-	39.0%	3.9%	-	45.0%	51.0	1.18
Ni4LA	13.6%	3.5%	43.5%	13.0%	3.0%	37.0%	4.1%	0.7%	44.7%	50.6	1.17
Ni14LA	13.6%	12.4%	38.0%	14.0%	9.5%	35.5%	3.0%	2.5%	40.3%	51.6	1.14
Ni37LA*	13.6%	32.7%	25.4%	20.5%	32.0%	15.5%	21.2%	13.2%	18.5%	45.6	1.11

For Ni37LA\* catalyst composition might be not representative for the inhomogeneities of the sample.

Table 3: Apparent reaction orders and activation energies for investigated NixLA catalysts

<b>catalysts</b>	<b>T [K]</b>	<b><math>\alpha</math></b>	<b><math>\beta</math></b>	<b><math>E_a</math> [kJ/mol]</b>	<b>Ref</b>
Literature Ni/Al <sub>2</sub> O <sub>3</sub> (20%wt)	523	0.32	0.16	83	[24]
Ni $\emptyset$ LA	523	0.41	0.20	73	This Study
Ni4LA	523	0.41	0.19	82	This Study
Ni14LA	523	0.45	0.12	78	This Study
Ni14LA	493	0.28	0.14		



## References

---

- [1] W. Wang, J. Gong, *Front. Chem. Sci. Eng.* 5 (2011) 2-10
- [2] G. Centi, S. Perathoner, *Catal. Today* 148 (2009) 191–205
- [3] M. Götz, J. Lefebvre, F. Mörs, A. McDaniel Koch, F. Graf, S. Bajohr, et al., *Renew. Energy*. 85 (2016) 1371–1390.
- [4] M. Bailera, P. Lisbona, L. M. Romeo, S. Espartero, *Renew. Sust. Energy Rev.* 69 (2017) 292–312
- [5] T.J. Schildhauer, S.M.A. Biolla, eds., *Synthetic Natural Gas: From Coal, Dry Biomass, and Power-to-Gas Applications*, Wiley, 2016.
- [6] D. Bellotti, M. Rivarolo, L. Magistri, A. F. Massardo, *Int. J. Hydrogen Energy*, 40 (2015) 2433-2444
- [7] M. S.Duyar, A. Ramachandran, C. Wang, R. J. Farrauto, *J. CO2 Utilization* 12 (2015) 27-33
- [8] X. Wang, Y. Hong, H. Shi, J. Szanyi, *J. Catal.* 343 (2016) 185–195
- [9] L. Falbo, M. Martinelli, C. G. Visconti, L. Lietti, C. Bassano, P. Deiana, *Appl. Catal. B: Environ.* 225 (2018) 354-363
- [10] G. Garbarino, P. Riani, L. Magistri, G. Busca, *Int. J. Hydrogen Energy* 39 (2014) 11557-11565
- [11] G. Busca, *Catal. Today* 226 (2014) 2-13.
- [12] G. Busca, *Advan. Catal.* 57 (2014) 319-404.
- [13] G. Busca, *Heterogeneous Catalytic Materials*, Elsevier, 2014, pp. 318-321.
- [14] S. Qi, X. Yong Wei, Z. Zong, Y. Wang, *RSC Adv.*, 3 (2013) 14219–14232.
- [15] Clariant, *Catalysts for syngas*, available on internet
- [16] Røstrup-Nielsen JR, Pedersen K, Sehested J, , *Appl. Catal. A: Gen.* (2007) 330 134-138.
- [17] I. Fechete, J.C. Vedin, B. Sels, M. Van de Voorde, eds., in *Nanotechnology in Catalysis: Applications in the Chemical Industry, Energy Development and Environmental protection*, Wiley, 2017, pp. 57-90.
- [18] C. Vogt, E. Groeneveld, G. Kamsma, M. Nachtegaal, Li Lu, C. J. Kiely, P. H. Berben, F. Meirer, B. M. Weckhuysen, *Nature Catalysis*, 1 (2018) 127–134.
- [19] G. Garbarino, C. Wang, I. Valsamakis, S. Chitsazan, P. Riani, E. Finocchio, M. Flytzani-Stephanopoulos, G. Busca, *Appl. Catal. B: Environ.* 174 (2015) 21-34.
- [20] S. Presto, A. Barbucci, M. P. Carpanese, M. Viviani, R. Marazza, *J Appl Electrochem* 39 (2009) 2257–2264 DOI 10.1007/s10800-009-9857-7
- [21] S. Kang, D. Lee, S. Kwon, *Aerospace Sci. Tech.* 46 (2015) 197–203
- [22] P. Alphonse, B. Faure, *Micropor. Mesopor. Mat.* 196 (2014) 191–198
- [23] I. Valsamakis, M. Flytzani-Stephanopoulos, *Appl. Catal. B: Environ.* 106 (2011) 255-263.
- [24] G. Garbarino, D. Bellotti, P. Riani, L. Magistri, G. Busca, *Int. J. Hydrogen Energy* 40 (2015) 9171-9182.

- 
- [25] G. Garbarino, C. Wang, I. Valsamakis, S. Chitsazan, P. Riani, E. Finocchio, M. Flytzani-Stephanopoulos, G. Busca, *Appl. Catal. B: Environ.* 200 (2017) 458–468
- [26] G. Garbarino, R.P. Parameswari Vijayakumar, P. Riani, E. Finocchio, G. Busca, *Appl. Catal. B: Environ.* 236 (2018) 490-500
- [27] “Pearson Crystal Data: Crystal structure database for inorganic compounds”, Release 2009/2012, ASM International, The Material Information Society
- [28] Levenspiel O, *Chemical Reaction Engineering*, 3rd ed., Wiley, New York, 1999, p.87.
- [29] Fogler HS, *Elements of Chemical Reaction Engineering*, fourth ed., Pearson Education International, New Jersey, 2006.
- [30] G. Busca, V. Lorenzelli, V. Sanchez Escribano, *Chem. Mater.* 4 (1992) 595-605
- [31] G. Garbarino, P. Riani, A. Infantes-Molina, E. Rodríguez-Castellón, G. Busca, *Appl. Catal. A: Gen.* 525 (2016) 180-189
- [32] G. Busca, P. Riani, G. Garbarino, G. Ziemacki, L. Gambino, E. Montanari, R. Millini, *Appl. Catal. A: Gen.* 486 (2014) 176-186.
- [33] G. Garbarino, S. Campodonico, A. Romero Perez, M. M. Carnasciali, P. Riani, E. Finocchio, G. Busca, *Appl. Catal. A: Gen.*, 452 (2013) 163-173.
- [34] G. Garbarino, I. Valsamakis, P. Riani, G. Busca, *Cat. Comm.* 51 (2014) 37-41
- [35] A.M. Hofmesiter, E. Keppel, A.K. Speck, *Mon. Not. R. Astron. Soc.* 345 (2003) 16-38.
- [36] M. Andrés-Vergés, C.J. Serna, *J. Mater. Sci. Lett.* 7 (1988) 970-972
- [37] V. Biju, M. Abdul Khadar, *Spectrochim. Acta Part A* 59 (2003) 121-134
- [38] M. Daturi, G. Busca, R.J. Willey, *Chem. Mater.* 7 (1995) 2115-2126.
- [39] B. Klingenberg, M.A. Vannice, *Chem. Mater.* 8 (1996) 2755–2768
- [40] R. Sarbajna, A.S. Devi, K. Purandhar, M.V. Suryanarayana. *Int. J. ChemTech Res.* 5 (2013) 2810-2820.
- [41] M. Gil-Calvo, C. Jiménez-González, B. de Rivas, J. I. Gutiérrez-Ortiz, R. López-Fonseca, *Appl. Catal. B: Environ.* 209 (2017) 128-138.
- [42] A. Tirsoaga, D. Visinescu, B. Jurca, A. Ianculescu, O. Carp, *J. Nanopart. Res.* 13 (2011) 6397-6408.
- [43] Y. Li, S. Yao, W. Wen, L. Xue, Y. Yan, *J. Alloys Compounds* 491 (2010) 560–564
- [44] C.E. Moffatt, B. Chen, D.M. Wieliczka, M.B. Kruger, *Solid State Commun.* 116 (2000) 631-636.
- [45] Y. Kameshima, A. Yasumori, K. Okada, *J. Surf. Sci. Soc. Jpn*, 21 (2000) 481-487.
- [46] F. S. Ohuchi, S. Ghose, M. H. Engelhard, D.R. Baer, *American Mineralogist*, 91 (2006) 740-746.
- [47] R. Lizarraga, E. Holmstrom, S. C. Parker, C. Arrouvel, *Physical Review B* 83 (2011) 094201.

- 
- [48] F. El Gabaly, K. F. McCarty, H. Bluhm, A. H. McDaniel, *Phys. Chem. Chem. Phys.*, 15 (2013) 8334-8341.
- [49] Xingkun Ning, Zhanjie Wang & Zhidong Zhang, *Scientific Reports* 5, Article number: 8460 (2015)
- [50] G. Vovk, X. Chen, C. A. Mims, *J. Phys. Chem. B* 109 (2005) 2445-2454.
- [51] M. Ferrandon, E. Björnbohm, *J. Catal.* 200 (2001) 148–159.
- [52] S. Mickevičius, S. Grebinskij, V. Bondarenka, B. Vengalis, K. Sliuziene, B.A. Orłowski, V. Osinniy, W. Drube, *J. Alloy. Compd.* 423 (2006) 107–111
- [53] Z. Boukha, L. Fitian, M. López-Haro, M. Mora, J.R. Ruiz, C. Jiménez-Sanchidrián, G. Blanco, J. J. Calvino, G. A. Cifredo, S. Trasobares, S. Bernal, 272 (2010) *J. Catal.* 121-130
- [54] J. Zheng, X. Ren, Y. Song, X. Ge, *React. Kinet. Catal. Lett.* 97 (2009) 109-114.
- [55] K. Ikkour, D. Sellam, A. Kiennemann, S. Tezkratt, O. Cherifi, *Catal. Lett.* 132 (2009) 213-217.
- [56] Ke Zhang, G. Zhou, J. Li, K. Zhen, T. Cheng, *Catal. Lett.* 130 (2009) 246–253.
- [57] E. Heracleous, A.F. Lee, K. Wilson, A.A. Lemonidou, *J. Catal.* 231 (2005) 159-171
- [58] P. Salagre, J.L.G Fierro, F. Medina, J.E. Sueiras, *J. Mol Catal A: Chem* 106 (1996)125-134
- [59] M.F. Sunding, K. Hadidi, S. Diplas, O.M. Løvvik, T.E. Norby, A.E. Gunnæs, *J. Electr. Spectr. Related Phenomena* 184 (2011) 399–408
- [60] K. Polychronopoulou, A.M. Efstathiou, *Catal. Today* 116 (2006) 341-347.
- [61] T.K. Phung, G. Garbarino, *J. Ind. Eng. Chem.* 47 (2017) 288-296
- [62] G.D. Weatherbee, C.H. Bartolomew, *J. Catal* 77 (1982) 460-472
- [63] F. Koschany, D. Schlereth, O. Hinrichsen *Applied Catalysis B: Environmental* 181 (2016) 504–516
- [64] D. Wierzbicki, R. Baranc, R. Dębek, M. Motak, M. E. Gálvez, T. Grzybek, P. Da Costa, P. Glatzel, *Appl. Catal. B: Environ.* 232 (2018) 409–419
- [65] D. E. Rivero-Mendoza, J.N. G. Stanley, J. Scott, K.-F. Aguey-Zinsou, *Catalysts* 6 (2016) 170; doi:10.3390/catal6110170
- [66] S. Rahmani, M. Rezaei, F. Meshkani, *J. Ind. Eng. Chem.* 20 (2014) 4176–4182
- [67] M. R. Gelsthorpe, K. B. Mok, J. R. H. Ross, R.M. Sambrook, *J. Mol. Catal.* 25 (1984) 253 - 262
- [68] D. Wierzbicki, R. Debek, M. Motak, T. Grzybek M.E. Gálvez, P. Da Costa *Catal. Commun.* 83 (2016) 5–8
- [69] V. Sanchez-Escribano, M.A. Larrubia Vargas, E. Finocchio, G. Busca, *Appl. Catal. A: Gen.* 316 (2007) 68–74.

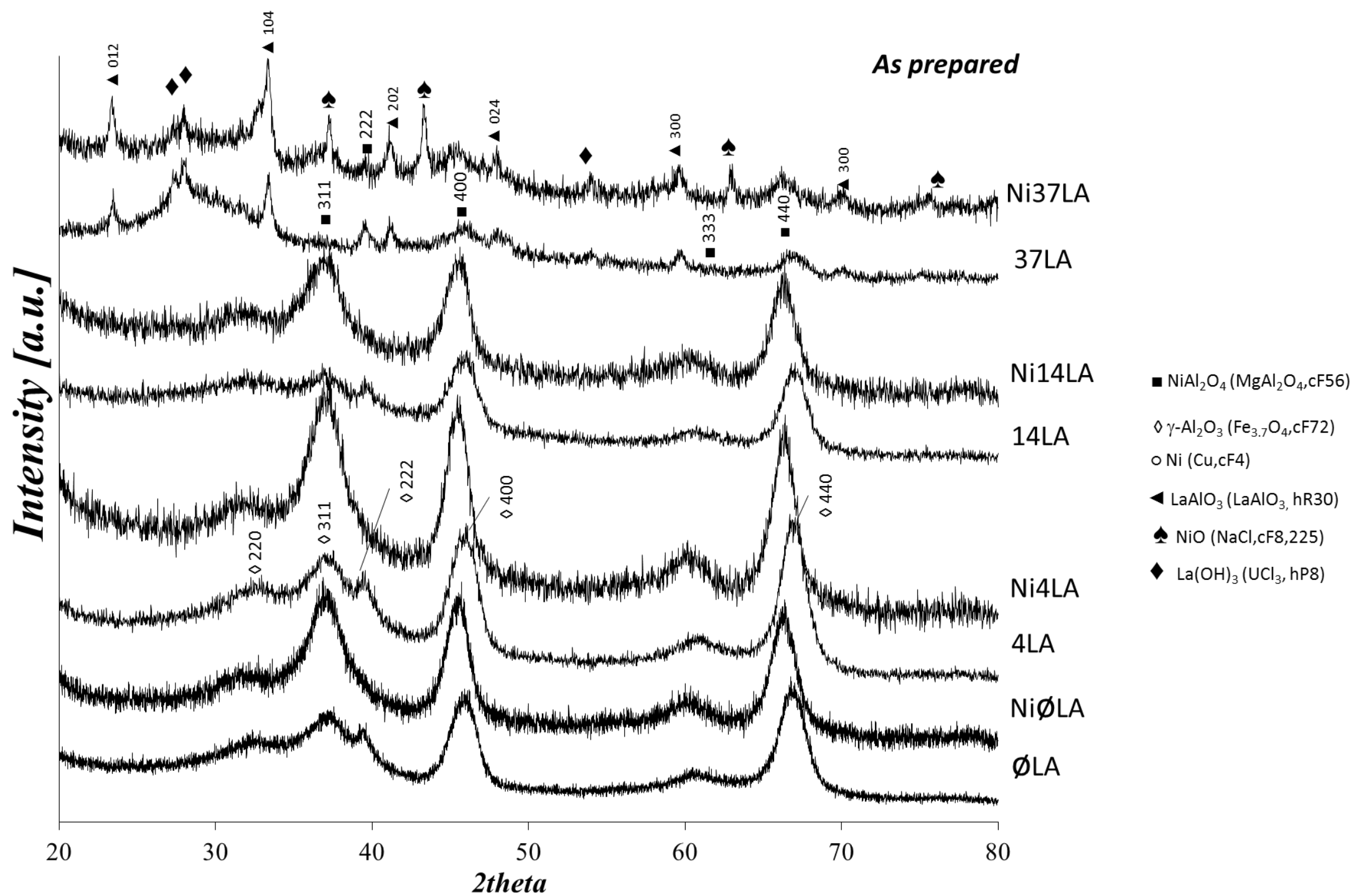


Figure 1



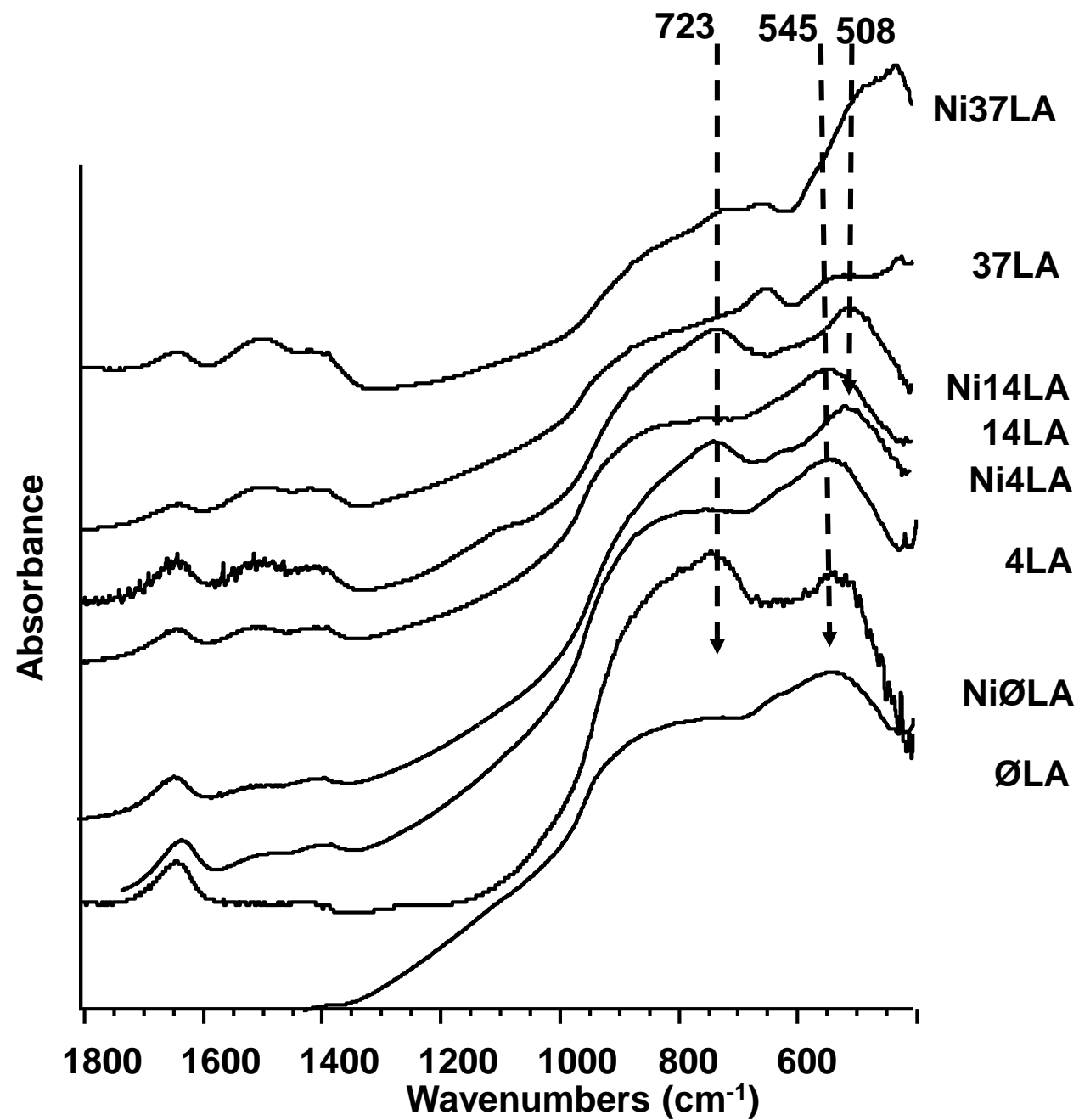


Figure 3

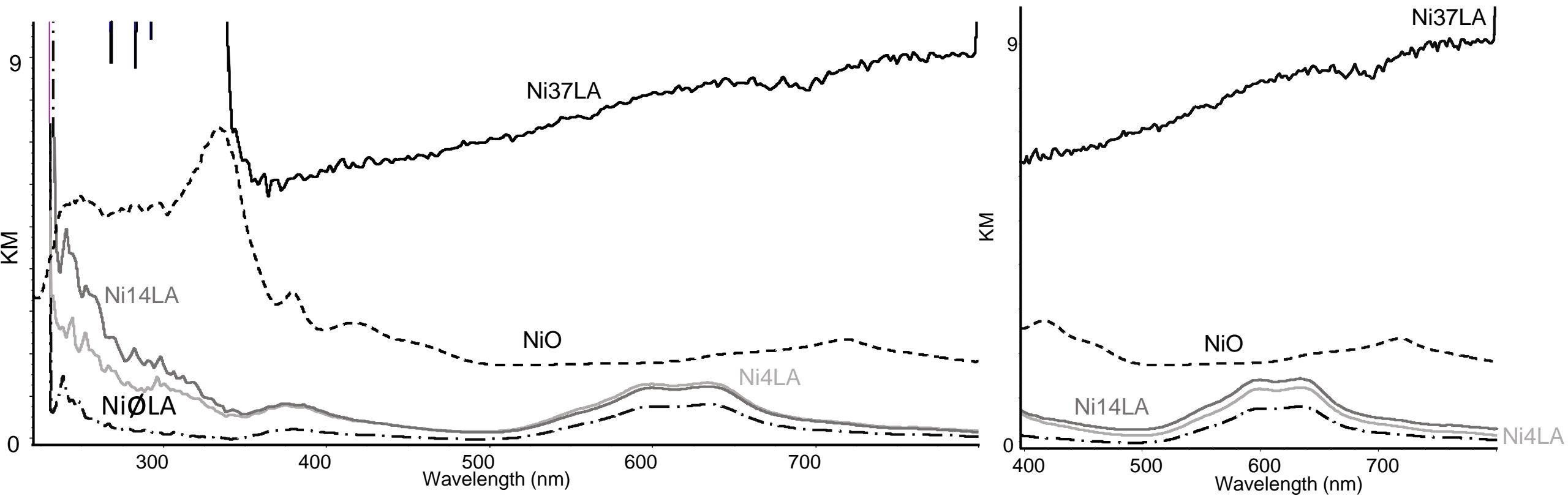
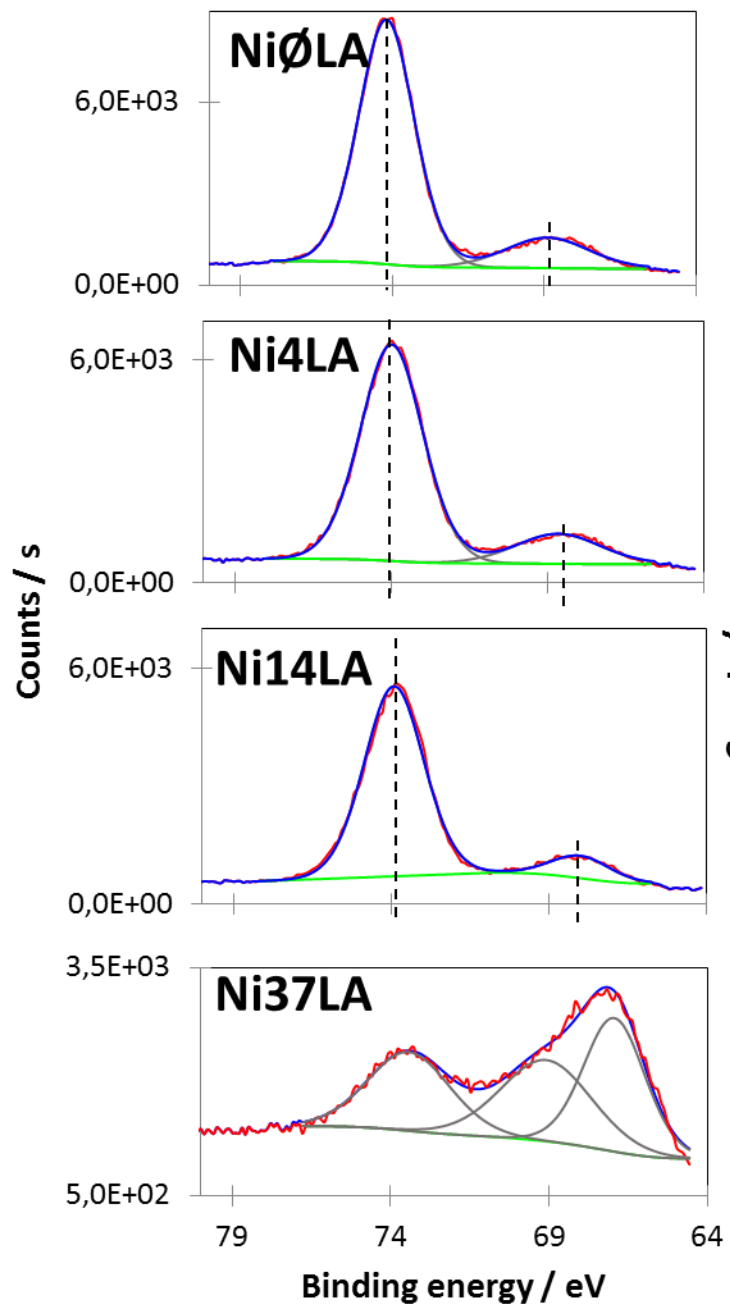


Figure 4

# Al (2p) & Ni(3p)



# La (3d 5/2)

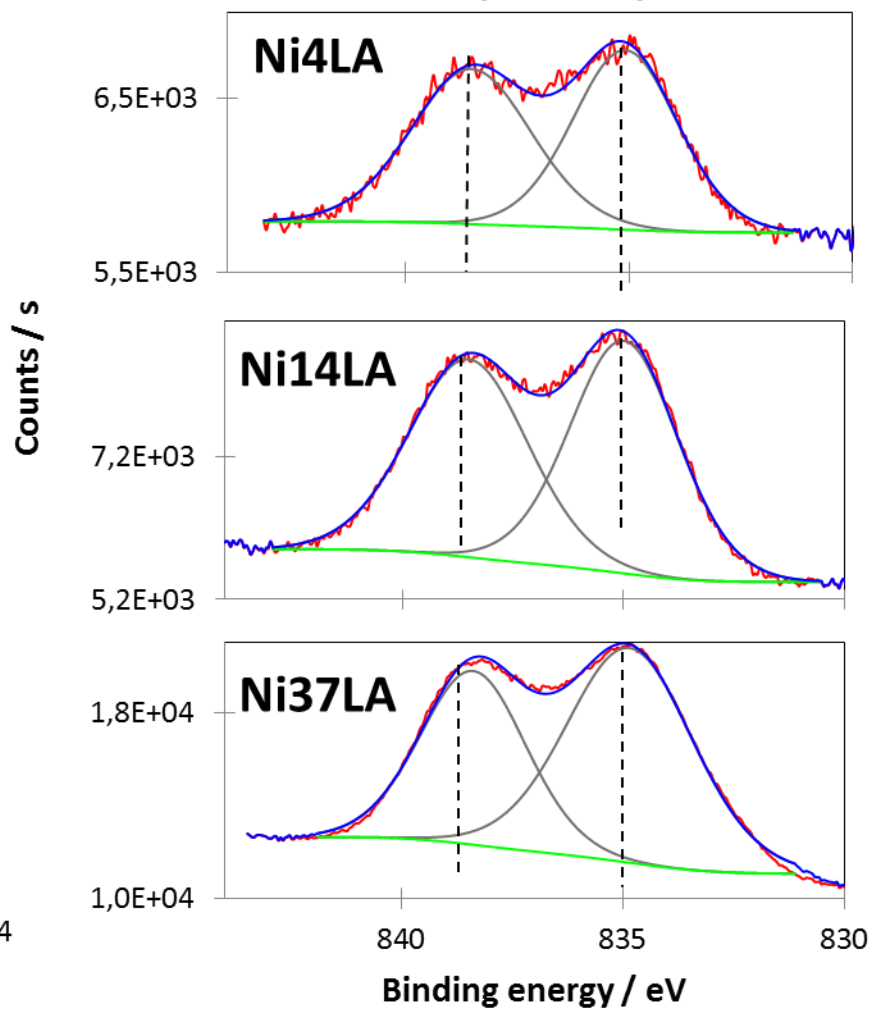


Figure 5

# Ni (2p 3/2)

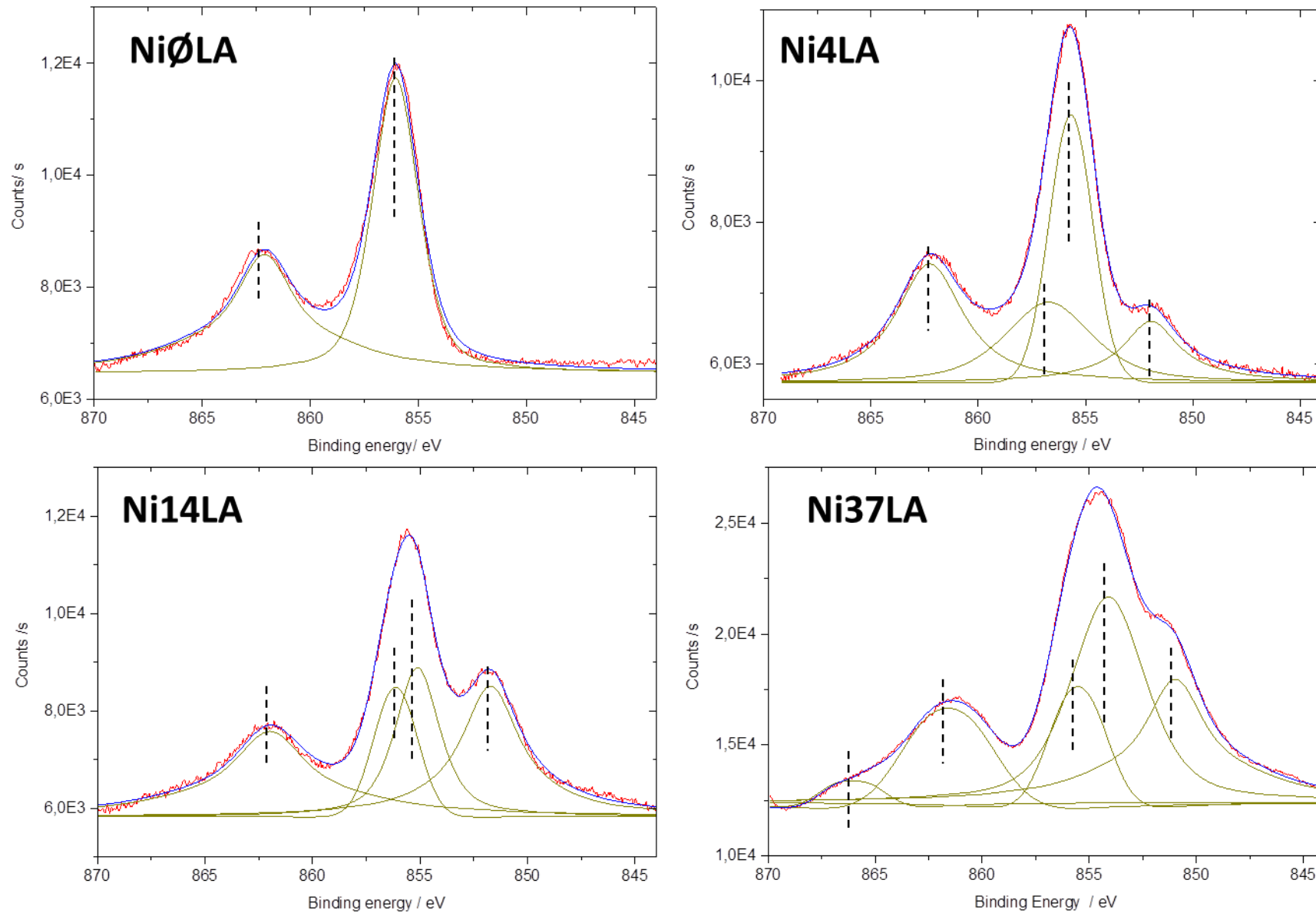


Figure 6

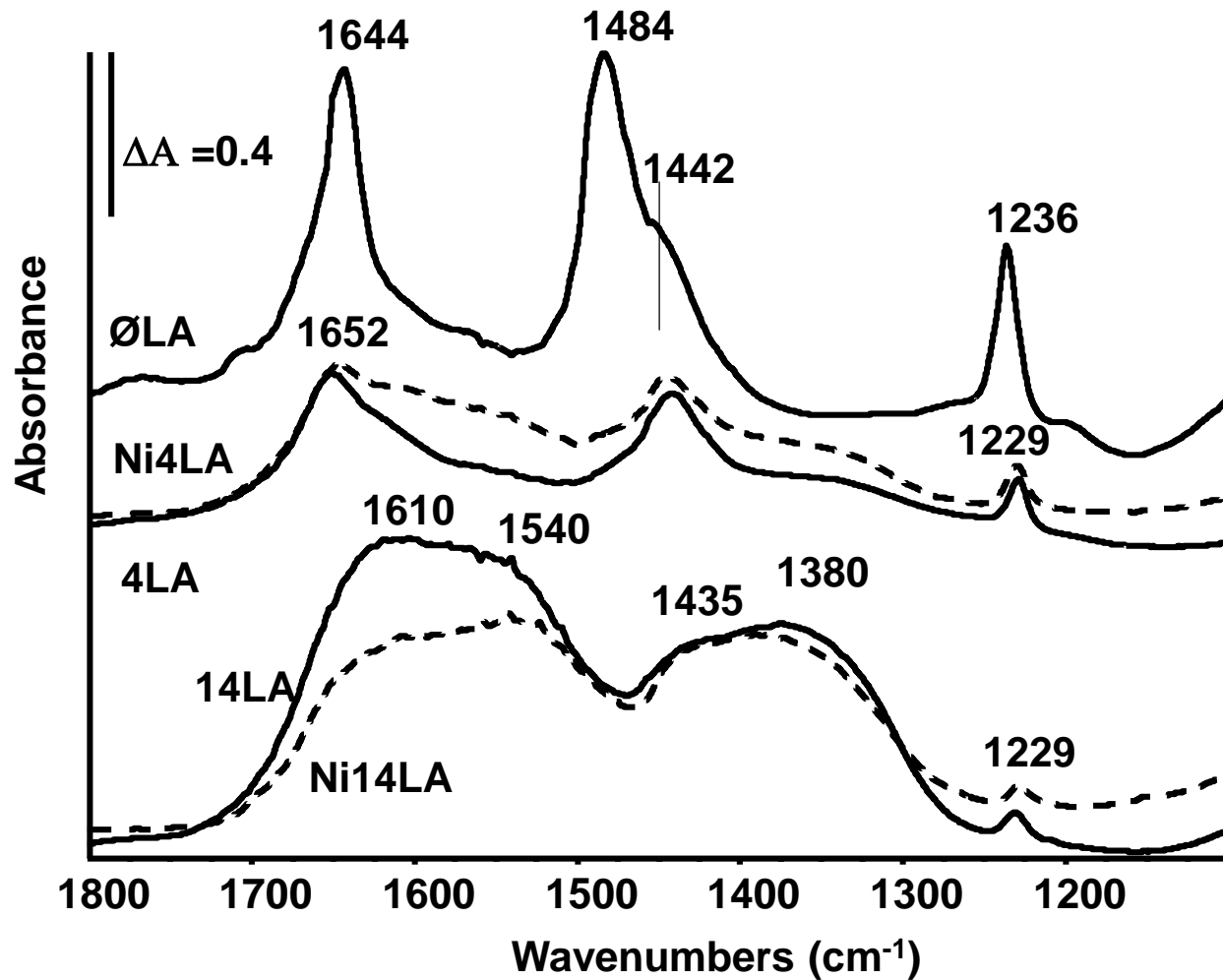
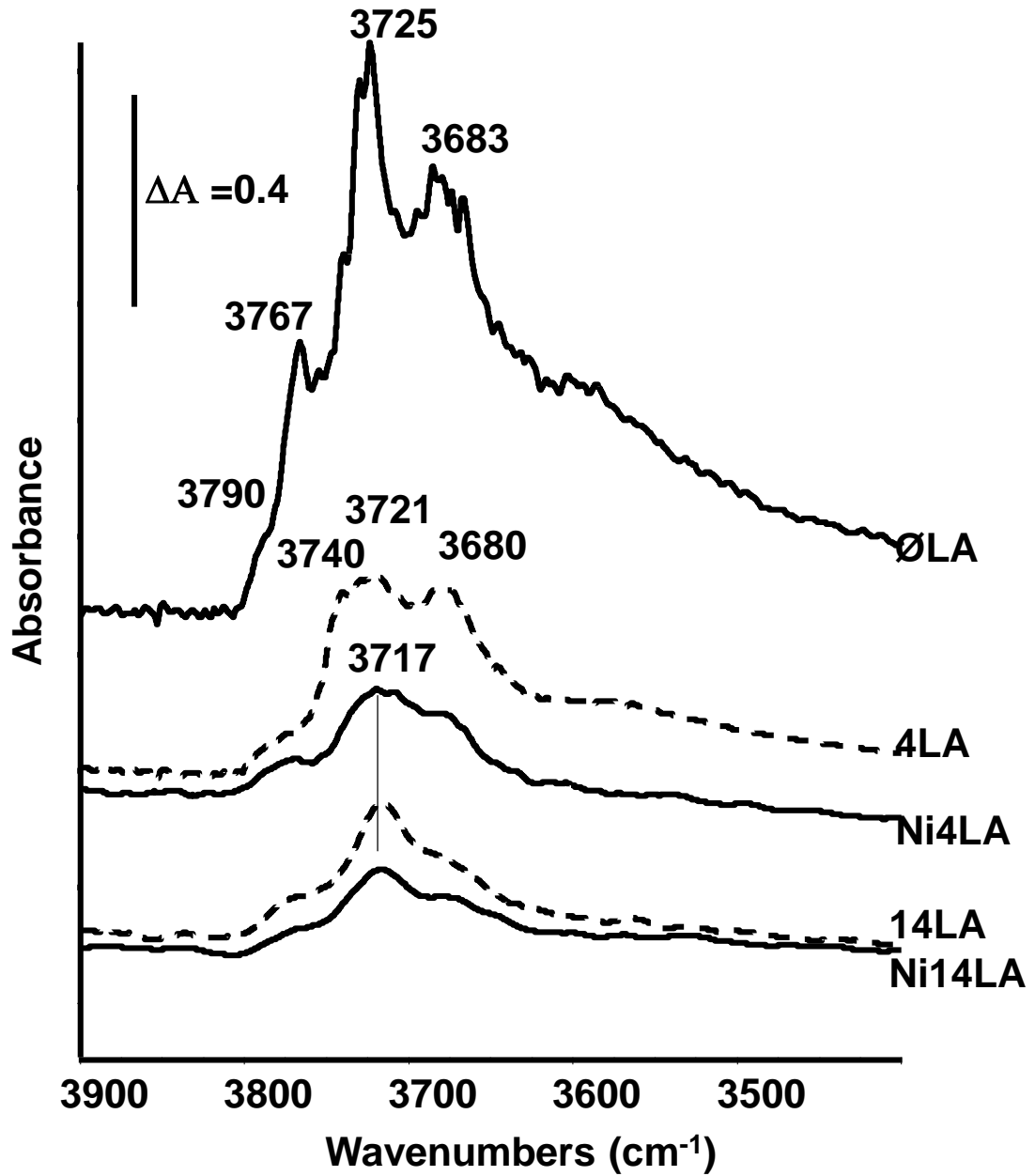


Figure 7

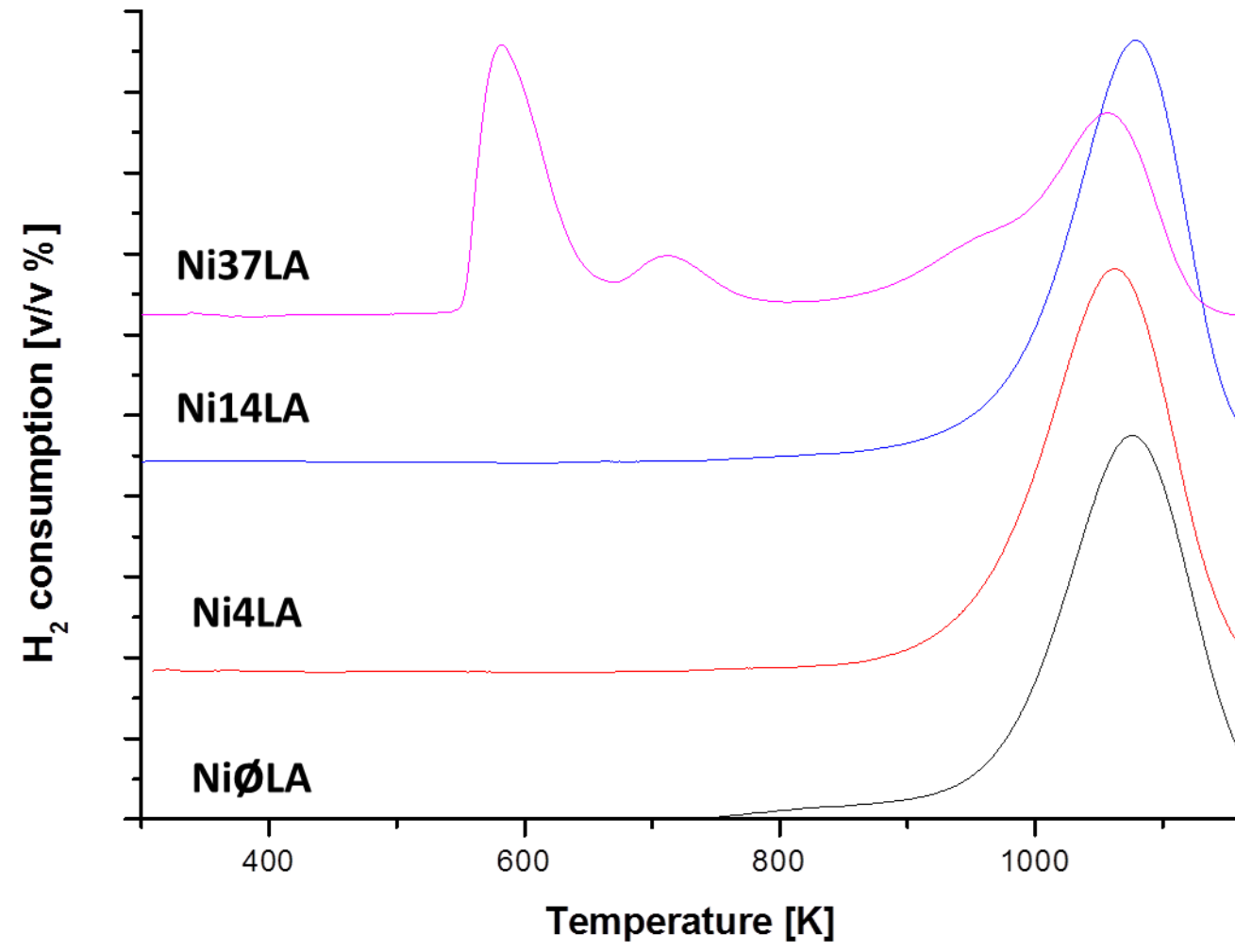


Figure 8

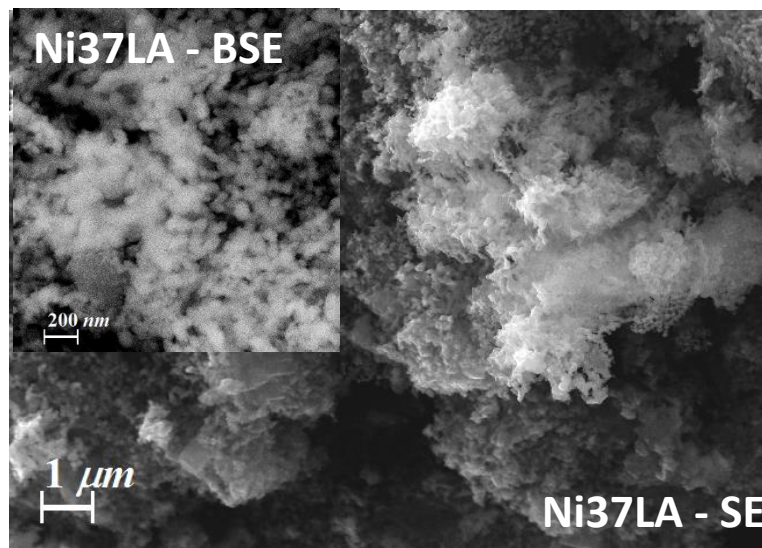
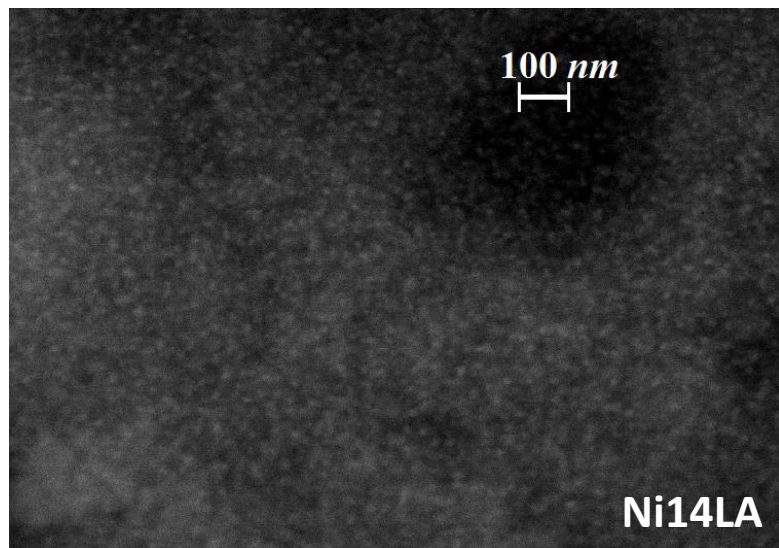
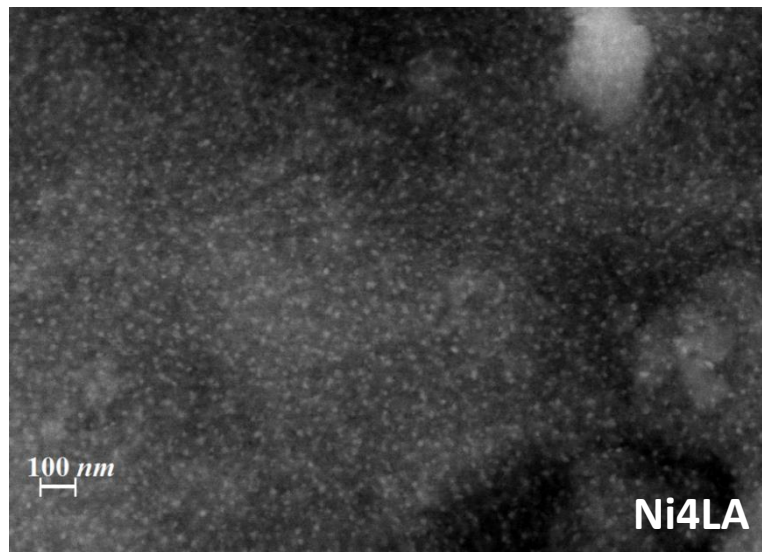
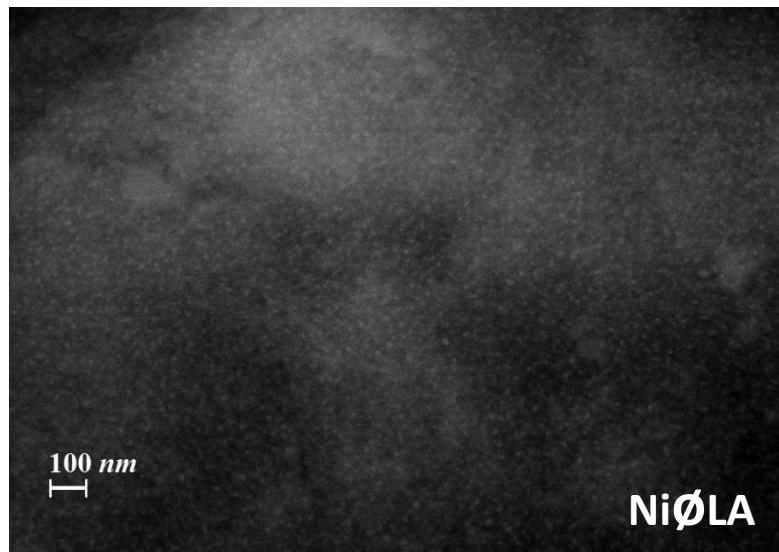


Figure 9

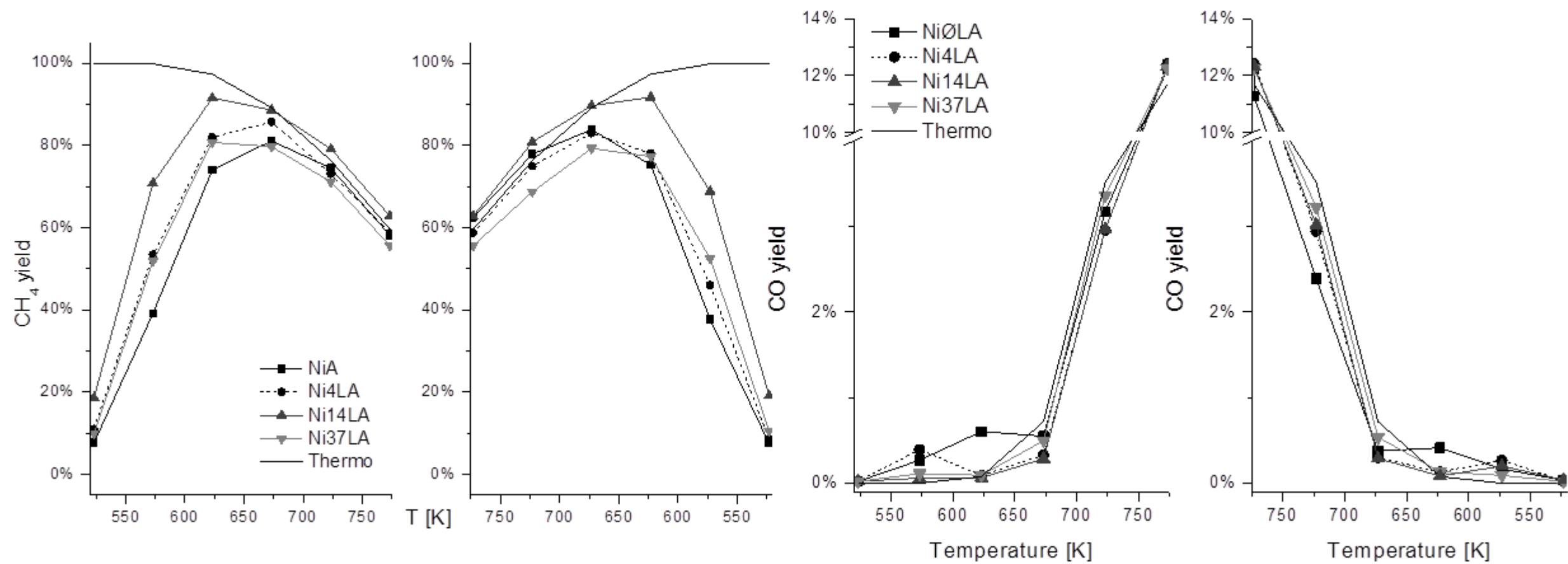


Figure 10

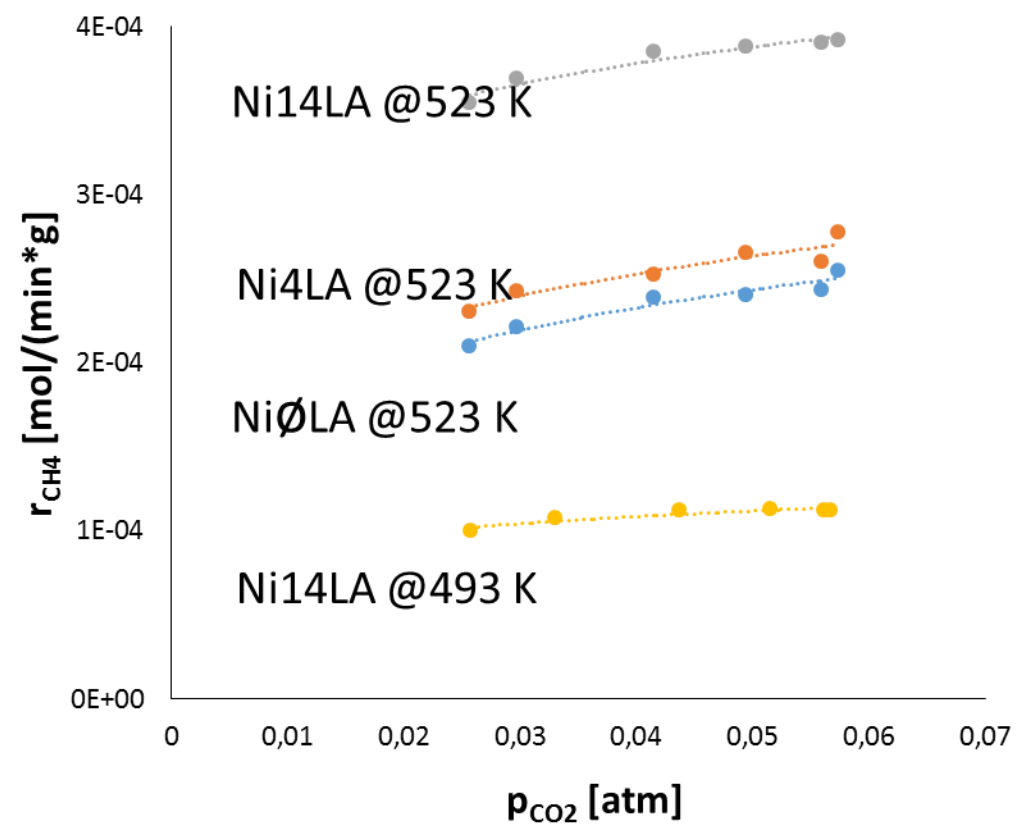
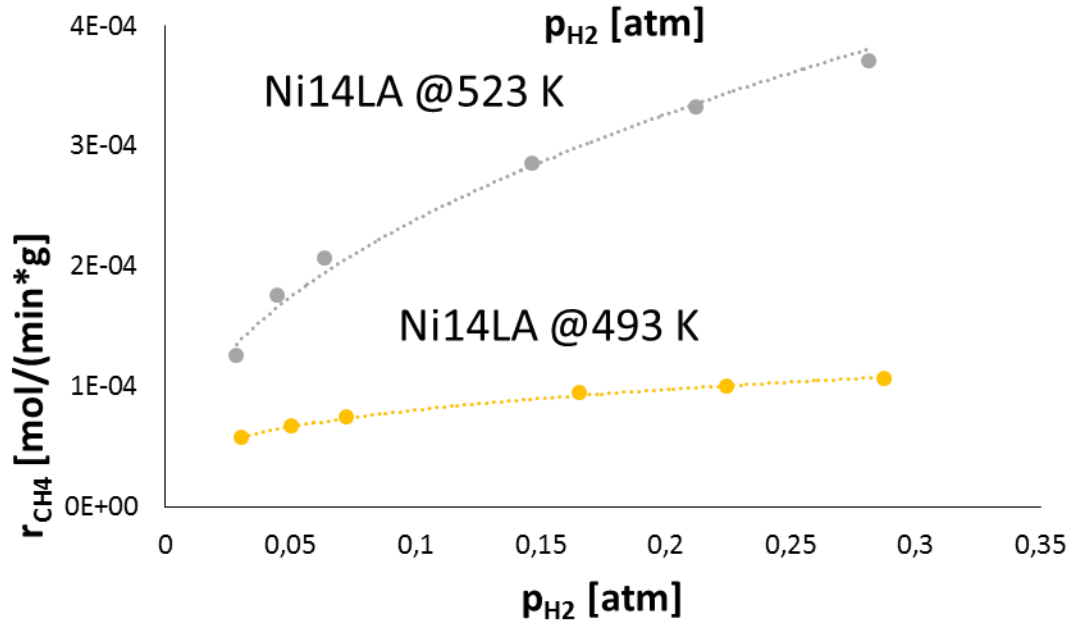
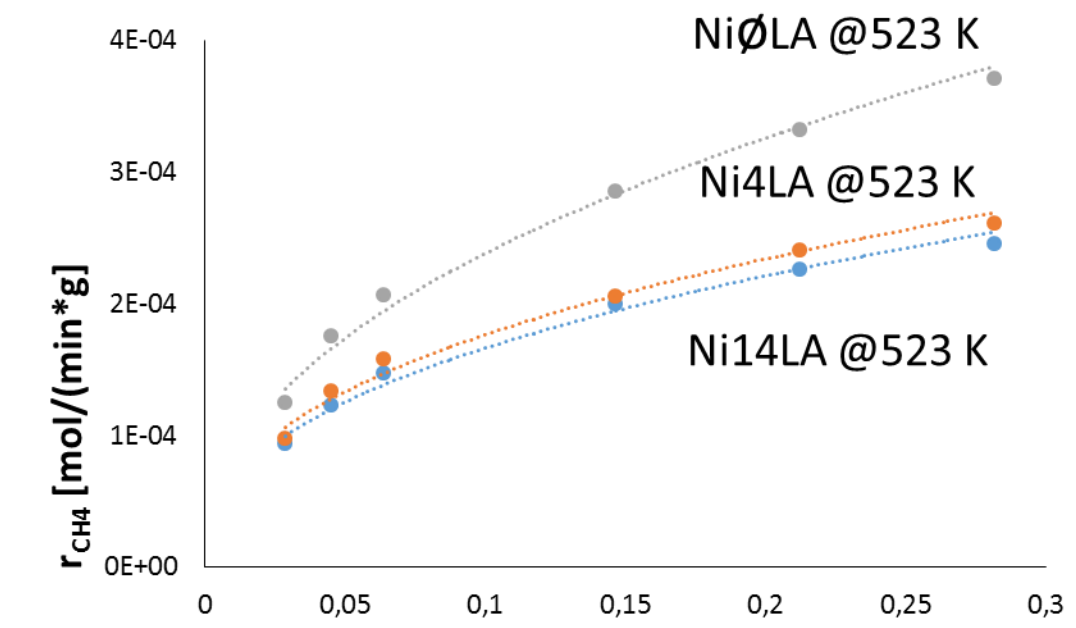


Figure 11

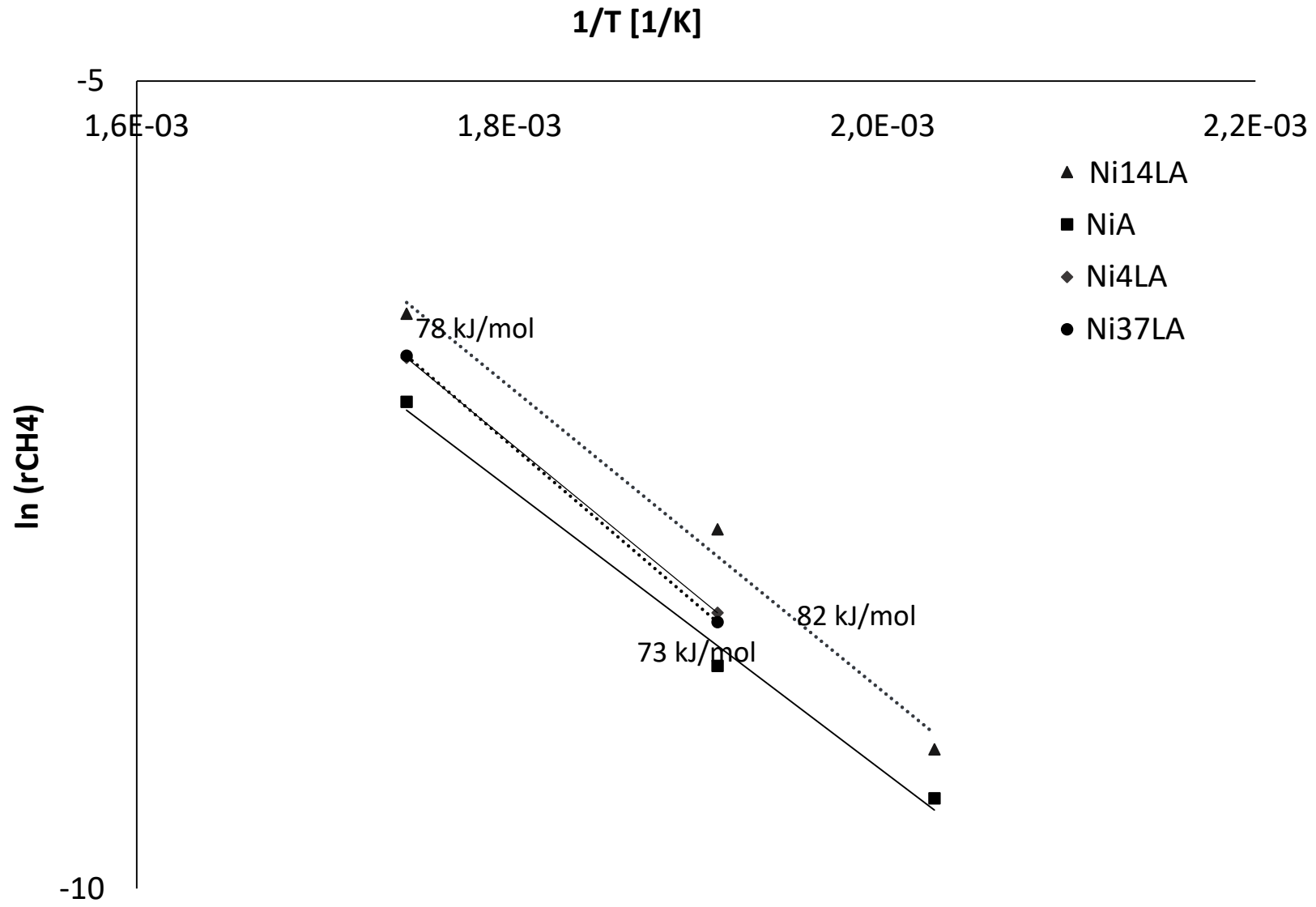


Figure 12